PEOPLES DEMOCRATIC REPUBLIC OF ALGERIA

MINISTRY OF HIGHER EDUCATION AND SCIENTIFIC RESEARCH

ECHAHID CHEIKH LARBI TEBESSI UNIVERSITY-TEBESSA

FACULTY OF EXACT SCIENCES AND THE SCIENCES OF NATURE

AND LIFE

DEPARTMENT OF MATTER SCIENCES

THESIS of MASTER

Specialty :Physics of Materials

Biological properties study of bioactive diopside containing 0.5wt% Na_2CO_3 prepared from local raw materials

Presented by:

LOUALI ROUFAIDA

Members of jury:

Dr. Khechba Mourad	**MCA**	President	Echahid Cheikh Larbi Tebessi
Dr. Zouai Souheila	**MCA**	Supervisor	Echahid Cheikh Larbi Tebessi
Dr. Belghit Hana	**MCB**	Examiner	Echahid Cheikh Larbi Tebessi

University season:2024/2025

Thesis Defense Date: June 10, 2025


بسم الله الرحمن الرحيم



Abstract:



This study initially focused on synthesizing diopside **($CaMgSi_2O_6$)** using the solid-state sintering method, starting with locally sourced dolomite **($CaMg(CO_3)_2$)** and low-cost laboratory-grade silicon dioxide **(SiO_2)**. The preparation process was carried out at a temperature of 1250°C for two hours through two mechanisms: one without additives and the other with the addition of 0.5% sodium carbonate. The sintered samples were characterized using X-ray diffraction **(XRD)** and Fourier-transform infrared spectroscopy **(FTIR)**. Results demonstrated an improvement in crystallization and sintering behavior with the addition of sodium carbonate **(Na_2CO_3)** , reflecting enhanced sintering performance. It was also confirmed that sodium was incorporated into the diopside without forming any secondary phases (Bioactive glasses).

Following the synthesis, the samples were crushed and subjected to bioactivity testing. This evaluation involved immersing diopside granules in simulated body fluid **(SBF)** for varying durations to examine the initiation and growth of apatite on their surfaces. The effect of sodium carbonate **(Na_2CO_3)** on the biological properties of diopside was investigated by analyzing the chemical composition using FTIR after immersion periods of 4 hours, 1 day, 4, 7, and 11 days. The findings indicated distinct differences in the partial dissolution behavior of the diopside granules during the early stages of immersion between samples with and without sodium carbonate addition. This variability was attributed to the role of sodium cations as network modifiers, reducing surface resistance to degradation in physiological fluids. Consequently, sodium addition significantly enhanced apatite nucleation and accelerated the formation of carbonate hydroxyapatite layers on sample surfaces compared to those without additives.

Furthermore, the samples containing sodium carbonate exhibited greater apatite deposition compared to pure diopside counterparts. Therefore, the study concluded that sodium carbonate acts as a bioactivity enhancer in diopside, improving their biological performance, particularly in terms of bioactive properties.

Key words: *Diopside, Dolomite, Sintering, Sodium carbonate, Silicon dioxide, Simulated body fluid, Crystallization, Carbonate hydroxyapatite layers, bioactivity testing.*



Résumé:



Cette étude s'est initialement concentrée sur la synthèse de la diopside **($CaMgSi_2O_6$)** par la méthode de frittage à l'état solide, en utilisant de la dolomie **($CaMg(CO_3)_2$)** d'origine locale et du dioxyde de silicium **(SiO_2)** de qualité de laboratoire à faible coût. Le processus de préparation a été réalisé à une température de 1250°C pendant deux heures, selon deux approches : l'une sans additifs et l'autre avec l'ajout de 0.5 % de carbonate de sodium **(Na_2CO_3)** . Les échantillons frittés ont été caractérisés par diffraction des rayons X **(DRX)** et spectroscopie infrarouge à transformée de Fourier **(FTIR)**. Les résultats ont révélé une amélioration de la cristallisation et du comportement au frittage grâce à l'ajout de carbonate de sodium, traduisant une performance accrue du frittage. Il a également été confirmé que le sodium était incorporé dans la structure de la diopside sans formation de phases secondaires (Verres bioactifs).

Après la synthèse, les échantillons ont été broyés et soumis à des tests de bioactivité. Ces évaluations consistaient à immerger les granules de diopside dans un fluide corporel simulé **(SBF)** pendant des durées variables pour observer l'initiation et la croissance d'apatite sur leurs surfaces. L'effet du carbonate de sodium sur les propriétés biologiques de la diopside a été exploré en analysant, par FTIR, la composition chimique des échantillons après des périodes d'immersion de 4 heures, 1 jour, 4, 7 et 11 jours. Les résultats ont mis en évidence des différences significatives dans le comportement de dissolution partielle des granules de diopside aux premiers stades d'immersion, entre les échantillons avec ou sans ajout de carbonate de sodium. Cette variabilité a été attribuée au rôle des cations sodium en tant que modificateurs du réseau, diminuant ainsi la résistance de surface à la dégradation dans les fluides physiologiques. En conséquence, l'ajout de sodium a nettement favorisé la nucléation d'apatite et accéléré la formation de couches d'hydroxyapatite carbonatée sur les surfaces des échantillons, comparativement à ceux sans additifs.

De plus, les échantillons contenant du carbonate de sodium ont présenté une plus grande déposition d'apatite que leurs homologues constitués uniquement de diopside pure. Ainsi, l'étude a conclu que le carbonate de sodium agit comme un amplificateur de bioactivité pour le diopside, améliorant ses performances biologiques, notamment en termes de propriétés bioactives.

Les mots clés: *Diopside, Dolomie, Dioxyde de silicium, Frittage, Carbonate de sodium, Cristallisation, Fluide corporel simulé, Hydroxyapatite carbonatée, Tests de bioactivité.*





الملخص:

ركزت هذه الدراسة أولا على تحضير الديوبسايد ($CaMgSi_2O_6$) باستخدام طريقة التلبيد بالحالة الصلبة، بدءًا من الدولوميت ($CaMg(CO_3)_2$) المحلي المصدر وثنائي أكسيد السيلكون (SiO_2) المختبري منخفض التكلفة. إذ تمت عملية التحضير عند درجة حرارة 1250°C لمدة ساعتين بآليتين مختلفتين: إحداهما بدون أي إضافات والأخرى بإضافة كربونات الصوديوم (Na_2CO_3) بنسبة 0.5%. وُصفت العينات الملبدة باستخدام حيود الأشعة السينية (XRD) ومطيافية تحويل فوريه للأشعة تحت الحمراء (FTIR) .

أشارت النتائج إلى تحسن في سلوك التبلور والتلبيد بإضافة كربونات الصوديوم، مما يعكس أداءً معززًا للتلبيد. كما تم تأكيد دمج الصوديوم في الديوبسايد دون تكوين أي طور ثانوي (الزجاجيات الحيوية). بعد التحضير تم سحق العينات وأُخضعت لاختبار النشاط الحيوي. تضمن التقييم غمر حبيبات الديوبسايد في سائل الجسم المقلد (SBF) و هذا لفترات زمنية متفاوتة لدراسة تنوي ونمو الأباتيت على أسطحها. إذ تم التحقيق في تأثير كربونات الصوديوم على الخصائص البيولوجية للديوبسايد من خلال مراقبة التركيب الكيميائي باستُخدام تقنية تحويل فوريه للأشعة تحت الحمراء خلال فترات الغمر التي استمرت 4 ساعات ويوم واحد و4 و7 أيام و11 يومًا. فأشارت النتائج إلى تباين تام لسلوك الذوبان الجزئي لحبيبات الديوبسايد خلال المراحل الأولى من الغمر لكل من العينات من دون إضافة وبإضافة كربونات الصوديوم، الأمر الذي يمكن إرجاعه لعمل كاتيونات الصوديوم كمُعدِّلات للشبكة وبالتالي قلّلت إضافة الصوديوم من مقاومة السطح للتحلل في السوائل الفسيولوجية. مما حفز بشكل ملحوظ تنوي الأباتيت، وسرع تكوين طبقة هيدروكسي أباتيت-كربونات على أسطح العينات مقارنةً بالعينات من دون إضافة.

علاوة على ذلك أظهرت العينات المضاف لها كربونات الصوديوم كميات أكبر من الأباتيت المترسب مقارنةً بنظيراتها من الديوبسايد النقي. وعليه خلصت الدراسة إلى أن كربونات الصوديوم تعمل كمعزز للنشاط الحيوي في الديوبسايد، مما يُحسّن أداءه الحيوي، لا سيما من حيث خصائصه المتعلقة بالنشاط الحيوي.

الكلمات المفتاحية: الديوبسايد، الدولوميت، ثنائي أكسيد السيلكون، التلبيد، كربونات الصوديوم، التبلور، سائل الجسم المقلد، هيدروكسي أباتيت-كربونات، النشاط الحيوي.



ACKNOWLEDGEMENTS



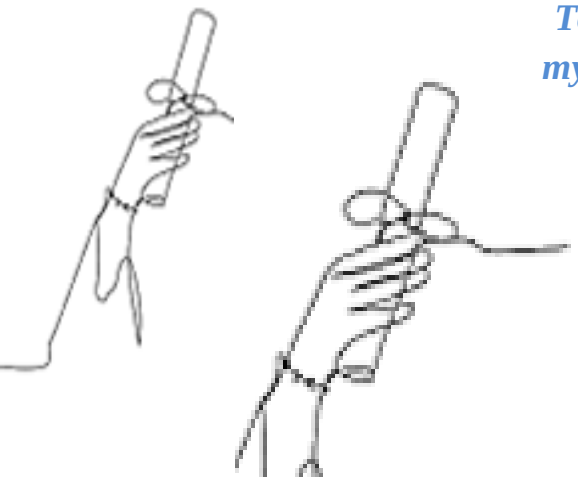
***P**raise be to **ALLAH** for guiding and assisting me in completing my graduation thesis, I am deeply grateful to him for his countless blessings and immense grace at every stage of my life. I pray that he continues to guide me in my future endeavours and keeps me always among the grateful.*

***I** would like to express my heartfelt gratitude to my supervisor **Dr.Zouai Souheila** for all her advice, guidance and support. I have learned much from her expertise in ceramics and bioceramics, and could always gain a lot of inspiration from her valuable comments and suggestions.*

***I** would like to express my sincere gratitude and deep appreciation to the members of the discussion committee, especially to **Dr.Khechba Mourad**, the chair of the committee, for his outstanding academic supervision and valuable guidance throughout the preparation of this thesis. I also extend my heartfelt thanks to **Dr.Belghit Hana** for her constructive contribution to the evaluation and discussion of the thesis, and for her insightful comments that greatly improved the quality of this work.*

***I** am also deeply grateful to my distinguished professors for their continuous support and encouragement throughout my academic journey — especially **Dr. Hafdallah Abdelkader**, whose generous guidance and valuable advice came at the times I needed them most.*

To all those who have helped me in my journey ,I hope that I have met your expectations.







DEDICATION



I praise and thank Almighty ALLAH for His grace and blessings, as His Kindness and Generosity have made this work possible.

Mom, your love has been my guiding star, leading me through life's ups and downs. Thanks you for always being there for me.Dear Mom, your sacrifices and prayers have made this achievement possible.

To my father,thank you for your wisdom, encouragement and the values you have instilled in me.Your strength and guidance have been my foundation.

To my sister NARIMANE, your Kindness and understanding have always been a source of encouragement.

To my brothers"ABDALLAH and MOUHAMED",thank you for your companionship and support. Your presence has made this academic journey more enjoyable.

This thesis is dedicated to all of you, with my deepest gratitude and love.



ROUFAIDA



List of contents

List of figures I

List of tables III

List of symbols IV

General introduction 02

Chapter I : Bibliographic studies of bioceramics and diopside

I .1. Overview of bioceramics 04

I.1.1. Definition 04

I.1.2. The Major Properties of Bioceramics 04

I.1.3. Classification of bioceramics 06

I.1.4. Apatite 07

1. Hydroxyapatite 07

2. Carbonate-containing Apatite 08

I.1.5. Bioceramics for medical applications 10

I .2. Overview of diopside 11

I.2.1. Definition 11

I.2.2. The Key Characteristics of diopside 12

I.2.3. Analysis of infrared spectroscopy 12

I.2.4. Synthesis methods of Diopside 19

I.2.5. FTIR analysis of diopside before and after SBF Immersion 21

I.2.6. Comparison between mechanical properties of diopside and human bone 21

I.2.7. Mechanism of interfacial bonding between bone tissue and diopside 23

I .3. Overview of sintering ……..……..……..……..... **23**

I.3.1. Definition ……..……..……..…….. **23**

I.3.2. Types of sintering process ……..……..…… **24**

I.3.3. Stages of Sintering ……..……..……. **24**

Chapter II : Elaboration and characterization of diopside

II .1. Experimental methods and materials

II .1.1. Overview of dolomite ….……..……..……... **26**

1. Definition ….……..……..……... **26**

2. The Key Properties of Dolomite ….……..……..……... **27**

3. Characterisation of dolomite ….……...…...……...……..……..... **29**

II .1.2. Silicon oxide SiO_2 ……...……..……...…..…… **30**

1. Definition ……..…….....…….....…... **30**

2. The Key Properties of SiO_2……...…. **30**

II .1.3. Addition: Sodium carbonate Na_2CO_3 …...…….……..……..…….... **31**

1. Definition …...……..……..……..….. **31**

2. The Key Properties of Sodium Carbonate …..……..…….. **31**

II .1.4. preparation of specimens..……..……...…… **32**

1. preparation of doloma ..……..…….. **32**

2. preparation of diopside ……..……..…..….. **33**

3. In Vitro Bioactivity Analysis ……..…….…….... **37**

II.2. Characterisation Techniques and Equipments

II .2.1. Characterisation Techniques ……..……..……..... **42**

II .2.2. Equipments ……..……...……..……..... **46**

List of contents

2025

Chapter III : Results and discussion

III-1 Structural properties before immersion in simulated body fluid (SBF).

III.1.1 Investigating the impact of adding 0.5 wt.% Na_2CO_3 on the crystallization **49**

III.1.2 Investigating the impact of adding 0.5% Na_2CO_3 on the sintering ……..….. **53**

III.1.3 Investigation the impact of adding 0.5% Na_2CO_3 on changes in chemical composition using (FTIR) spectroscopy ……..……..... **55**

III-2 In-vitro bioactivity assessment.

III.2.1 After immersion for 4 hours in SBF ……..... **56**

III.2.2 After immersion for 1day in SBF …… **58**

III.2.3 After immersion for 4 days in SBF ……..… **59**

III.2.4 After immersion for 7 days in SBF ……..…… **60**

III.2.5 After immersion for 11 days in SBF ……....……..… **63**

General conclusion ……..……..…… **65**

References……...……..…… **69**

List of figures

Figure N°	Title	Page
I.1	Examples of alumina/zirconia bioceramics for hip joint prosthesis and dentistry.	5
I.2	Solubility of some Ca-P compounds at 25°C (g/l) .	6
I.3	Crystallographic structure of hydroxyapatite showing the orthohexagonal unit Cell.	7
I.4	The used of bioceramic for dentistry.	9
I.5	Schematic CaO-SiO2-MgO system showing Diopside zone.	11
I.6	Structure of Diopside (Monoclinic).	12
I.7	the wavenumbers of FTIR spectra for natural diopside	12
I.8	A diagram illustrating the experimental steps for preparing diopside using the sol-gel method.	13
I.9	XRD patterns of diopside ceramics after immersion in SBF for 3, 7,14 and 21 days	14
I.10	FTIR spectra of diopside ceramics (a) before and (b) after immersion in SBF for 14 days.	15
I.11	SEM-EDS of diopside ceramics (a) before (b) after 14 days and (c) after 21 days of immersion in SBF.	16
I.12	A diagram illustrating the experimental steps using the Solid-State Reaction method.	17
I.13	XRD pattern of diopside sintered at 1300 °C (a) before, (b) after soaking in the SBF.	18
I.14	FTIR spectra of diopside powders (a) before, (b) after 2 days, and (c) after 21 days of immersion in SBF.	18
I.15	SEM images of the obtained diopside powders sintered at 1300 °C for 2 hours: (a) before, (b) after 2 days, and (c) after 21 days of immersion in SBF.	19
I.16	Schematic representation of the apatite-forming mechanism on the surface of Diopside in SBF.	22
I.17	Schematic illustration of the normal bone remodeling process.	23
I.18	Types of sintering process.	24
I.19	Different stages of sintering.	24
II.1	Crystal Structure of dolomite.	27
II.2	Ternary Phase Diagram of Carbonate Minerals ($CaCO_3$–$MgCO_3$–$FeCO_3$ System).	27
II.3	DTA curve of a local dolomite stone sample.	28

II.4	FTIR analysis of natural dolomite.	29
II.5	Crystal Structure of SiO_2.	30
II.6	Amorphous Structure of SiO_2.	30
II.7	Crystal Structure of Na_2CO_3.	31
II.8	(XRD) patterns of **(a)** raw dolomite **(01)** dolomite cal (doloma) **(02)** doloma hyd **(03)** doloma hyd cal **(b)** silicon oxide.	33
II.9	Experimental Procedure for Preparing doloma.	34
II.10	(XRD) patterns of **(01)** after grinding and **(02)** after grinding followed by calcination.	35
II.11	Experimental Procedure for Preparing diopside samples.	36
II.12	Experimental Procedure for Preparing SBF.	40
II.13	Preparation and Weighing of Crushed Diopside Samples. (The weight here is divided by 6).	41
II.14	Diopside samples after immersion in SBF and subsequent drying.	41
II.15	Crushing device.	42
II.16	A precision balance of the " SHIMADZU AUW 220D" type.	43
II.17	Automatic incubator type " Egg Incubator 96 Eggs ".	43
II.18	Magnetic heater.	44
II.19	pH Meter.	44
II.20	FT/IR-4X Fourier Transform Infrared (FTIR) Spectrometer.	45
II.21	XRD spectrometer.	45
II.22	Electric oven type " NABERTHERM ".	46
II.23	A mechanical compactor of the Specac type.	46
III.1	DTA curve of pure diopside samples.	48
III.2	XRD spectra of pure diopside and diopside doped with 0.5 wt.% Na2CO3, calcined at 740°C for 2 h.	49
III.3	XRD spectra of pure diopside and diopside doped with 0.5 wt.% Na2CO3, sintred at 1250 °C for 2 h.	50
III.4	XRD spectra of pure diopside showing peak broadening for crystallite size estimation.	51
III.5	XRD spectra of doped diopside showing peak broadening for crystallite size estimation.	52

III.6	FTIR spectra of both sintered undoped (a) and doped with 0.5 wt.% Na_2CO_3 (b) samples prior to their immersion in the SBF solution.	55
III.7	FTIR spectra of the sintered, undoped (a) and doped with 0.5 wt.% Na_2CO_3 (b) samples after immersion for 4 hours in the SBF.	57
III.8	FTIR spectra of the sintered, undoped (a) and doped with 0.5 wt.% Na_2CO_3 (b) samples after immersion for 1 day in the SBF.	58
III.9	FTIR spectra of the sintered, undoped (a) and doped with 0.5 wt.% Na_2CO_3 (b) samples after immersion for 4 days in the SBF.	59
III.10	FTIR spectra of the sintered, undoped (a) and doped with 0.5 wt.% Na_2CO_3 (b) samples after immersion for 7 days in the SBF.	61
III.11	FTIR spectra of the sintered, undoped (a) and doped with 0.5 wt.% Na_2CO_3 (b) samples after immersion for 11 days in the SBF.	62

List of tables

Table N°	Title	Page
I.1	The Key Properties of hydroxyapatite.	8
I.2	The wavenumbers of FTIR spectra for CHA synthesized at various temperatures.	9
I.3	Key Properties of $CaMgSi_2O_6$ (Diopside).	12
I.4	Wavenumbers of FTIR spectra for diopside synthesized at 800°C.	15
I.5	Wavenumbers of FTIR spectra for diopside synthesized at 1300°C before and after soaking in the SBF.	19
I.6	FTIR Spectral Data of Diopside Samples Synthesized by Different Methods Before and After SBF Immersion.	20
I.7	Comparison between mechanical properties of diopside and human bone.	21
II.1	Important Properties of Dolomite.	27
II.2	Chemical composition of the dolomite stone used .	28
II.3	Vibrational frequency assignments (FT–IR).	30
II.4	Important Properties of SiO2 (Silicon dioxide).	30
II.5	Important Properties of Na_2CO_3 (**S**odium carbonate).	31
II.6	Ion concentration in SBF and human blood plasma.	37
II.7	Components required for the preparation of simulated body fluid (SBF).	38
III.1	Mechanical and Structural Properties of Diopside samples sintred at 1250 °C for 2 h	53

List of symbols

Symbols	Signification
FAP	Fluorapatite
HAP/HA	Hydroxyapatite
β-TCP	β -Tricalcium phosphate
α-TCP	α-Tricalcium phosphate
OCP	Octacalcium phosphate
DCPD	Dicalcium phosphate dihydrate, mineral brushite
CaPs	Calcium phosphates
PMS	Polymethylsiloxane
SEM	Scanning Electron Microscopy
DP	Diopside
ICDD	International Centre for Diffraction Data
SBF	Simulated Body Fluid
FTIR	Fourier Transform Infrared Spectroscopy
XRD	X-Ray Diffraction
EDS	Energy Dispersive X-ray Spectroscopy



GENERAL INTRODUCTION

General introduction

The universe is undoubtedly under the complete control of the Great Creator, Allah. Allah brought everything in existence, from humans and animals to plants, soil, air, water, and beyond. It is affirmed that everything was created from water. Regarding the creation of humans, Allah crafted all things with great precision and excellence. The initial stage of human creation was shaped from clay. This process is also described in the Quran, specifically in verse 14 of Surah Ar-Rahman.

"خَلَقَ الإِنْسَانَ مِنْ صَلْصَالٍ كَالفَخَّارِ"
"He created man from clay like [that of] pottery."

Clays represent one of the most significant rocks on Earth and serve as a fundamental raw material widely utilized in the production of various ceramic products. The history of ceramic production can be traced back to the early stages of human development. Over time, advancements in technology have led to the development of specialized ceramics, which have played a crucial role in innovative applications such as the repair or replacement of diseased or damaged body parts. These advancements have significantly improved the quality of life and, in some cases, even extended life expectancy for countless individuals, particularly during the latter decades of the 20th century. Such materials, known as bioceramics, are specifically designed for applications in the musculoskeletal system. They can be categorized based on their biological interactions, including bioinert options (e.g., alumina and zirconia), resorbable materials (e.g., tricalcium phosphate), and bioactive substances (e.g., hydroxyapatite, bioactive glasses, glass-ceramics, and diopside).

Within this context, diopside has gained recognition as a promising bioceramic material, offering significant benefits in various medical applications. Diopside ($CaMgSi_2O_6$) is a calcium silicate-based material renowned for its bioactive properties. Additionally, it possesses notable physical characteristics, such as high hardness and tensile strength, which further enhance its suitability as a bioceramic. In terms of bioactivity, diopside demonstrates a moderate capacity to induce apatite layer formation under laboratory conditions and supports bone growth in vivo. However, there is potential for improvement to maximize its effectiveness and reliability. To address these challenges, researchers have explored incorporating additives as an innovative strategy. The inclusion of additives has been shown to enhance diopside's bioactive performance, promote its sintering processes, improve its mechanical properties, and increase its antibacterial resistance.

This study focuses on synthesizing diopside ceramics using locally available raw materials through the solid-state sintering method. A key objective is to investigate the impact of adding 0.5 wt.% sodium carbonate (Na_2CO_3) on the crystallization behavior and sintering performance of the diopside samples. Additionally, this research evaluates how this additive influences the material's bioactivity by examining its ability to form apatite layers when immersed in simulated body fluid. To characterize the prepared samples, various analytical techniques were employed, with particular emphasis on X-ray diffraction (XRD) and Fourier-transform infrared spectroscopy (FTIR).

The research is organized into three chapters as follows:

Chapter I: presents a literature review addressing bioceramics, the properties and synthesis of diopside, and the sintering method.

Chapter II: details the raw materials, experimental procedures, and analytical techniques utilized in this study, including FTIR and XRD.

Chapter III: focuses on analyzing and discussing the experimental results derived from the investigation of bioceramics.



CHAPTER I

BIBLIOGRAPHIC STUDIES OF BIOCERAMICS AND DIOPSIDE

I - Bibliographic Studies of Bioceramics and Diopside

I .1. Overview of bioceramics :

The opening section of Part 01 in this chapter provides a clear and concise definition of bioceramics. Subsequent discussions delve into the diverse and extensive aspects of bioceramics science, covering topics such as their classifications, as well as their physical, biological, and chemical properties....

I.1.1. Definition:

The term **bioceramics** is a combination of two components: **"ceramics,"** derived from the Greek word "keramikos," meaning "of pottery," and "bio," signifying its interaction with living tissue. A ceramic refers to an inorganic, non-metallic solid, typically composed of oxides, nitrides, borides, or carbides, and formed through high-temperature firing [4].

I.1.2. The Major Properties of Bioceramics :

Bioceramics are classified based on their properties, and among the most important of these properties, we mention the following :

- ✓ **Mechanical properties**: The latest generation of bioceramics is designed to stimulate the body's natural self-repair mechanisms. As a result, the goal during restoration is for mature bone to replace the existing implants seamlessly, ensuring this transition occurs without any temporary loss of mechanical support, , which requires maintaining essential mechanical properties such as hardness, tensile strength, and flexural resistance throughout the healing process [5].

- ✓ **Biological properties:** Bioceramics are widely utilized as bone grafts due to their favorable biological properties, such as bioaffinity, biocompatibility, bioactivity, osteoinduction, osteointegration, and osteoconduction [6].

- ✓ **Chemical properties:** One of the most considerable mechanisms accelerating material aging is chemical corrosion. Generally, bioceramics are considered highly resistant to chemical corrosion [7].

I.1.3. Classification of bioceramics : **B**oth ideologically and historically, the study of bioceramics can be partitioned in to the first, second and third generations **[5].**

➢ 1st generation: (Bioinert ceramics):

Bioinert ceramics are a type of bioceramic classified based on their interaction with biological systems in the human body. Unlike some other materials, bioinert ceramics do not trigger significant immune responses and are highly resistant to corrosion, enhancing their integration and compatibility with bodily tissues. Additionally, these materials are non-toxic and free from harmful or adverse effects.

The most commonly used bioinert ceramics include Zirconia (ZrO_2) **(Fig.I.1)**, Alumina (Al_2O_3) **(Fig.I.1)**, and various forms of Silicon Nitride (Si_3N_4) **[8,9]**.

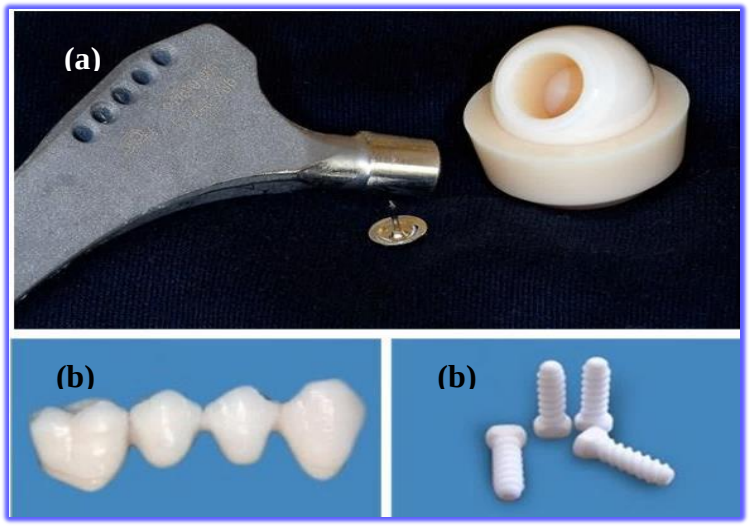


Fig.I.1. Examples of (a) alumina/(b) zirconia bioceramics for hip joint prosthesis and dentistry **[10].**

➢ 2nd generation: (Bioactive and the Bioresorbable):

✓ **Bioactive ceramics:** This category of bioceramics has the ability to integrate seamlessly with living tissues after implantation, promoting osteogenesis. However, due to their fragility, they are primarily employed to fill small bone defects and correct periodontal irregularities. Notable examples include wollastonite ($CaSiO_3$), hydroxyapatite ($Ca_{10}(PO_4)_6(OH)_2$), Nevertheless, certain bioceramics, such as diopside (CaMgSi2O6), exhibit acceptable bioactivity along with favorable mechanical properties.… **[10].**

✓ Bioresorbable ceramics:

Certain materials are gradually absorbed within the body and replaced by bone over time. Examples of such materials include calcium carbonates ($CaCO_3$), calcium silicates ($CaSiO_3$), and calcium phosphates (CaPs). Among these, calcium phosphates stand out due to their ideal calcium-to-phosphorus (Ca/P) ionic ratio **(Fig.I.2)**, which makes them particularly well-suited for biomedical applications. However, only specific compounds are viable for implantation, as those with a Ca/P ionic ratio below 1 are unsuitable because of their high solubility **[10.11].**

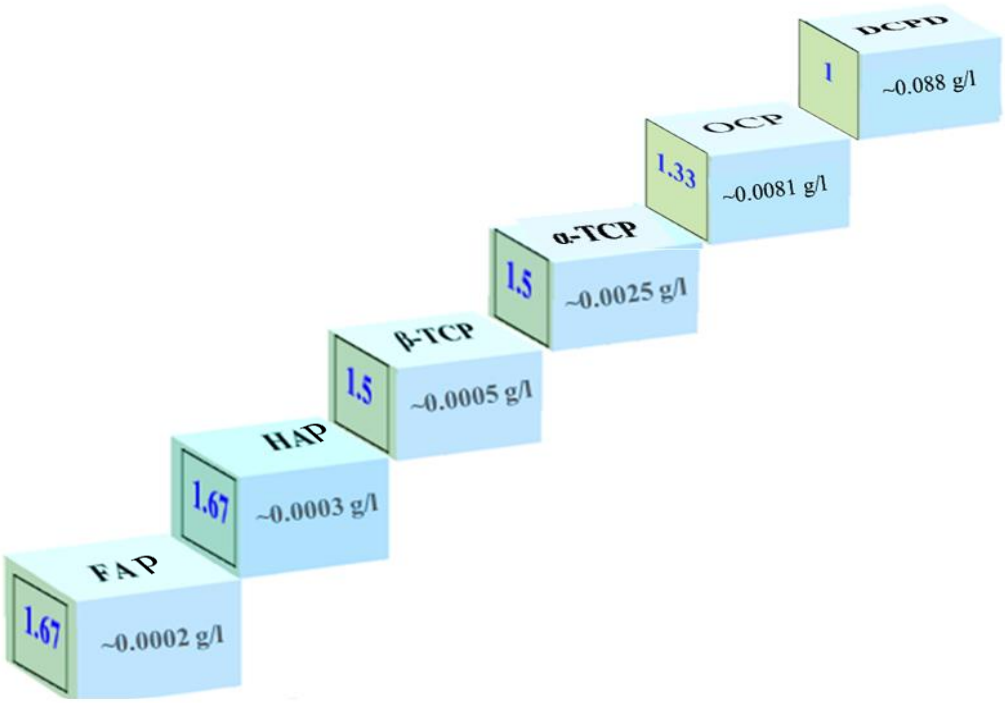


Fig.I.2. Solubility of some **Ca-P** compounds at 25C° (g/l) **.**

➢ **3rd generation: (Porous bioceramics):** Porous ceramics generally refer to ceramic materials with a porosity exceeding 30%. These ceramics can be synthesized from a range of nonmetallic inorganic materials, such as ceramic powders, or from organic materials like polymer precursors, including PMS. Achieving a porosity between 20% and 27% is relatively straightforward; however, specialized techniques are necessary to create ceramics with exceptionally high porosity. Porous ceramic technologies have been implemented in industries across Russia and other countries since the year 1930. Typically, both pore size and porosity in these materials can vary considerably, with sizes ranging from 1 to 700 micrometers and porosity levels spanning from 15% to 95%. These variations largely depend on the type, size, volume fraction of the template, and the specific forming technology used **[3].**

I.1.4. Apatite: Apatite is a bio-ceramic material that chemically resembles human bone and is used as a bone substitute to promote the formation of new bone. It is one of the most abundant naturally occurring minerals on Earth, found in igneous, metamorphic, and sedimentary rocks. Its chemical formula is $Ca_5(PO_4)_3(F^-,Cl^-,OH^-,CO_3^{2-})$, represented by variations such as Hydroxyapatite (HAp, $Ca_{10}(PO_4)_6(OH)_2$), Fluorapatite (FAp, $Ca_{10}(PO_4)_6F_2$), Chlorapatite (ClAp, $Ca_{10}(PO_4)_6Cl_2$), and Carbonate-containing Apatite (CAP, $Ca_{10}(PO_4)_6(CO_3)$).

1. Hydroxyapatite: Hydroxyapatite is an important inorganic material prominently used as a substitute for bones and teeth. Its bioceramic surface closely resembles approximately 60-70% of the mineral composition found in human bone. Composed of calcium, phosphorus, and hydroxyl ions, which enhances its exceptional biocompatibility and bioactivity in various biomedical applications hydroxyapatite exhibits a densely packed hexagonal crystalline structure **(Fig. I.3)**. As part of the calcium phosphate (CaP) family, it incorporates diverse phosphate-based anions, such as orthophosphate, metaphosphate, or pyrophosphate, along with hydrogen or hydroxyl ions. In its pure form, hydroxyapatite appears as a white powder; however, natural samples can display colors like yellow, brown, or green due to the presence of impurities. With its structural and chemical similarity to human hard tissues, hydroxyapatite is gaining attention for its potential in addressing age-related conditions such as osteoporosis, making it an area of growing scientific interest and research focus **[6,12]. Table I.1** highlights the primary attributes of hydroxyapatite.

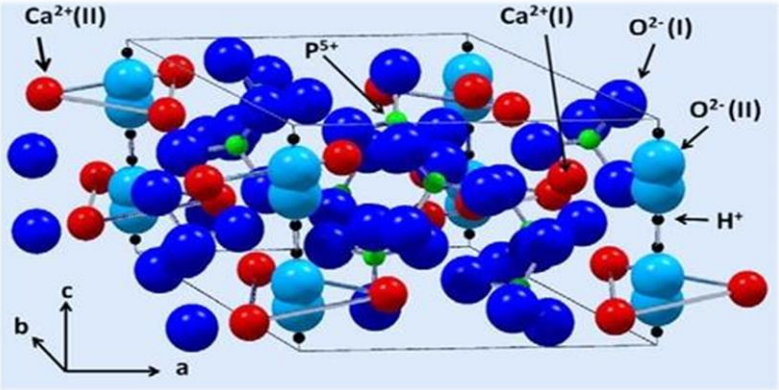


Fig.I.3. Crystallographic structure of hydroxyapatite showing the orthohexagonal unit cell with**: a=9.432A°, b=a√3, c=6.8814A°, γ=120° and β = α= 90° [13].**

Table. I.1. The Key Properties of hydroxyapatite.

Properties		Ref
Name	Hydroxyapatite	**/**
Compound	HA or HAp	/
Chemical Formula	$Ca_{10}(PO_4)_6(OH)_2$	/
Ca/P	1.67	**[6]**
Young's modulus (GPa)	35 to 120 (dense HA)	**[11]**
Solubility in water	Poorly soluble in water	
Onset of thermal decomposition (°C)	1100 – 1300	**[14]**

2. Carbonate-containing Apatite: The substitution of carbonate in the crystal lattice of hydroxyapatite can occur either at hydroxyl or phosphate sites, identified as type A and type B, respectively. Previous studies have generally described carbonate-substituted hydroxyapatite as type B, based on infrared and X-ray data. Some research papers document the effects of two deposition variables temperature and bicarbonate ion concentration—on the morphology, phase composition, and calcium, phosphorus, and carbon content of the deposited carbonate hydroxyapatite. Variations in temperature and bicarbonate concentration can result in either needle-like or spherical crystals. Infrared spectroscopy indicated that carbonate occupies site A at low carbonate content (<4%). At higher carbonate content (>4%), the carbonate is predominantly found at site B. **Table. I.2** provides the wavenumber values (cm^{-1}) of the FTIR spectra for carbonated hydroxyapatite (CHA) synthesized at various temperatures **[15].**

Table. I.2. The wavenumbers of FTIR spectra for CHA synthesized at various temperatures **[15].**

CO_3^{-2} ν_2	PO_4^{-3} ν_1	PO_4^{-3} ν_3	CO_3^{-2} ν_3
875	960	1059,1086	1534,1557,1574 1420,1454,1488
875	961	1041,1084	1418,1456,1557
873	961	1048,1063	1419,1539,1557
871	960	1008,1050	1473,1489,1505 1419,1434,1457
872	960	1052	1473 > 1488,1505 1419,1433,1457 >
875	961	1061,1090	1419,1556,1488
873	961	1042	1419,1456,1488
872	961	1045	1419,1456,1473
872	961	1046	1419,1557,1473
875	962	1049,1090	1419,1455
874	961	1040,1087	1419,1455
873	961	1042	1417,1454
873	961	1052	1418,1456
873	961	1039	1413 > 1450,1467
875	962	1035,1093	1420,1455

I.1.5. Bioceramics for medical applications:

✓ Bioceramic in dentistry:

Bioceramics play a vital role in modern dentistry, enhancing the quality of advanced implants and restorative solutions **(Fig.I.4)** like crowns, inlays, and dentures **[17].**

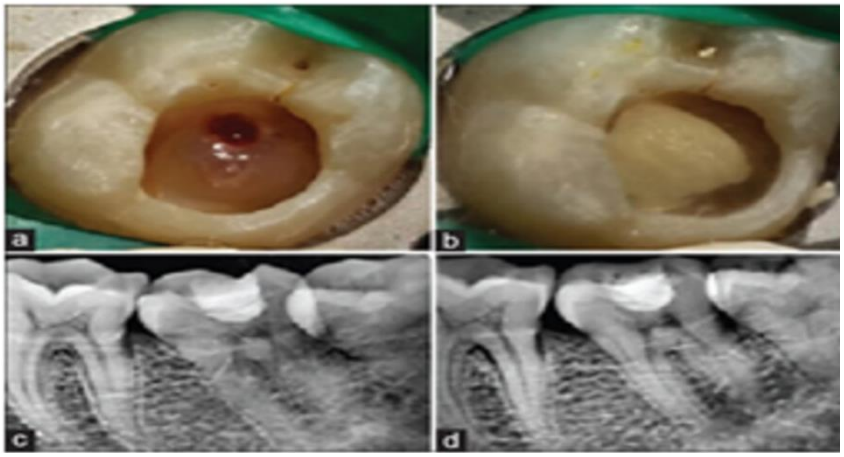


Fig.I.4. The used of bioceramic for dentistry **[16].**

✓ Bioceramics as Drug Delivery Systems:

Calcium phosphate-based bioceramics are extensively utilized in drug delivery applications due to their excellent biocompatibility, osteoconductivity, and osteoinductivity. Their high porosity allows for substantial drug loading and controlled release; however, this feature weakens their mechanical strength, limiting their suitability for addressing large bone defects. As an alternative, diopside ($CaMgSi_2O_6$) has gained attention for its superior mechanical properties, bioactivity, and controlled biodegradability. Diopside shows promise for localized drug delivery, particularly in the treatment of conditions such as osteosarcoma and glioblastoma. Using bioceramic scaffolds for local drug delivery reduces systemic side effects and enhances targeting of residual tumor cells following surgical interventions. Additionally, spheroid-based three-dimensional cell cultures offer a more precise in vitro model to evaluate the impact of drug release. Diopside particles have demonstrated the ability to effectively adsorb and gradually release doxorubicin, exerting selective cytotoxic effects on tumor spheroids. These systems represent a promising approach for localized, sustained anticancer therapy **[18].**

✓ 3D-Printed custom implants:

One prominent area benefiting from 3D-printed bioceramics is the advancement of artificial hip joints used in orthopedic surgeries. Patients undergoing hip joint replacement procedures present unique morphological challenges for medical professionals. Hip joints are intricate three-dimensional structures that require extensive customization to align with the patient's specific anatomy. Currently, operating rooms rely on a range of predefined shapes and sizes to accommodate variations in hip structures **[17].**

I .2. Overview of diopside:

This section explores diopside as a bioactive ceramic material, focusing on its classification, essential properties, and synthesis methods. The discussion highlights key characterization techniques, including XRD, SEM, and FTIR, to understand its bone-bonding behavior. By comparing diopside's performance with natural bone, the analysis demonstrates its potential for bone tissue engineering and regenerative medicine applications.

I.2.1. Definition :

Diopside ($CaMgSi_2O_6$) is a silicate mineral belonging to the pyroxene group with a monoclinic crystal structure **(Fig. I.6)**. Historically valued as a gemstone, its name derives from the Greek words "di," meaning "two" or "double," and "opsis," signifying "appearance" or "look," likely referencing its optical properties such as birefringence or pleochroism. Diopside is typically found in a range of colors, including colorless, white, yellow, pale to dark green, or black, and it displays a white to gray-green streak and a vitreous to dull luster. Its theoretical oxide composition consists of 55.55% SiO_2, 25.98% CaO, and 18.51% MgO. In the CaO–SiO_2–MgO ternary phase diagram **(Fig. I.5)**, diopside occupies a distinct stability region. This region is surrounded by other phases like Akermanite, Pseudo-Wollastonite, Protoenstatite, Forsterite, and Periclase, highlighting the specific conditions under which diopside forms in high-temperature silicate systems **[18,19].**

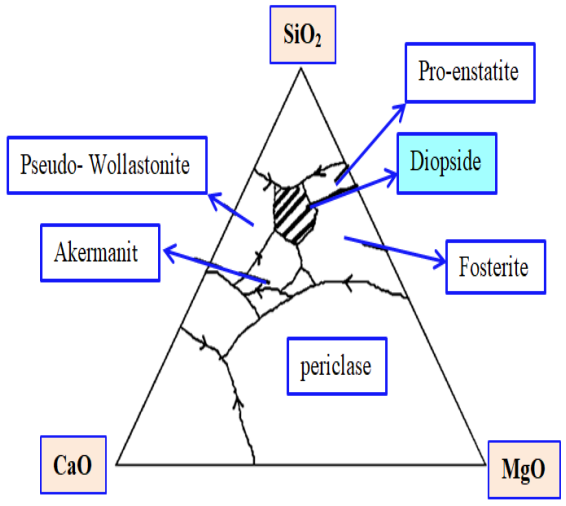


Fig. I.5. Schematic CaO-SiO2-MgO system showing Diopside zone. **[20]**

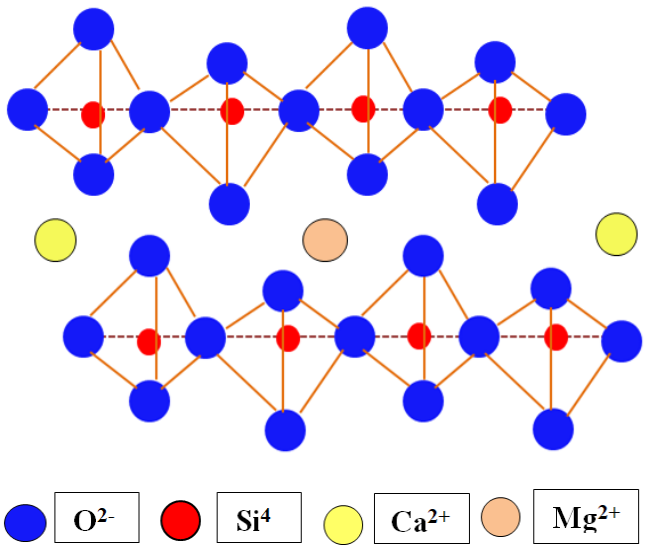


Fig. I.6. Structure of Diopside (Monoclinic) with cell parameters**: a=9.76 A°, b=8.899 A°, c=5.251A°, β =74.17 ° and γ= α= 90° [20]**

I.2.2. The Key Characteristics of Diopside: Diopside ceramics are defined by a range of unique properties, the most notable of which are outlined in **Table I.3**.

Table. I.3. Key Properties of $CaMgSi_2O_6$ (Diopside).

Properties		Ref
Name	Diopside	/
Compound	DP	/
Chemical Formula	$CaMgSi_2O_6$	/
density (g/cm3)	~ 3.2	**[21]**
Fracture toughness ($MPa \cdot m^{1/2}$)	~ 3.5	
Young's modulus (GPa)	170	
Melting Point (°C)	T_f = 1391	**[22]**

I.2.3. Analysis of infrared spectroscopy : The FTIR spectroscopy analysis of natural diopside is presented in this section **(Fig. I.7)** and will be compared against experimental results.

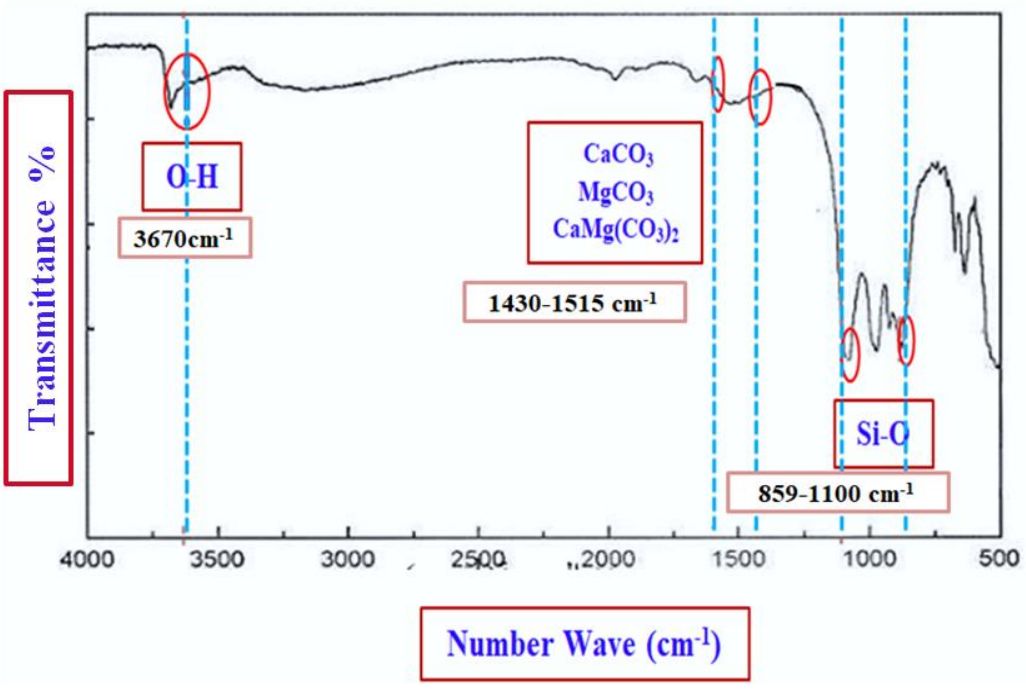


Fig. I.7 the wavenumbers of FTIR spectra for natural diopside **[23].**

I.2.4. Synthesis methods of Diopside :

The various processes employed for the synthesis of Diopside are:

- Co precipitation process
- Solid-State reaction
- Sol-Gel process

} are employed for the preparation of dense bulk solids.

- Spray pyrolysis → is used for preparation of thin films.

In our current study, the diopside has been synthesized by solid-state reaction process at a sintering temperature 1250 °C for 2 hours . Therefore, we have selected two previously studied methods to compare their results with those obtained in the present work.

➢ **Sol-Gel:** The Sol-Gel method is a sophisticated chemical process utilized in the production of bioceramics. It involves converting solutions into a gel, which is subsequently subjected to thermal treatment. This approach facilitates the creation of exceptionally pure and uniform nanomaterials, making it particularly well-suited for biomedical applications like bone and dental implants.

✓ **Method :** The diagram **(Fig. I.8)** outlines the key experimental procedures for synthesizing diopside via the sol-gel method at a sintering temperature of 800°C **[24].**

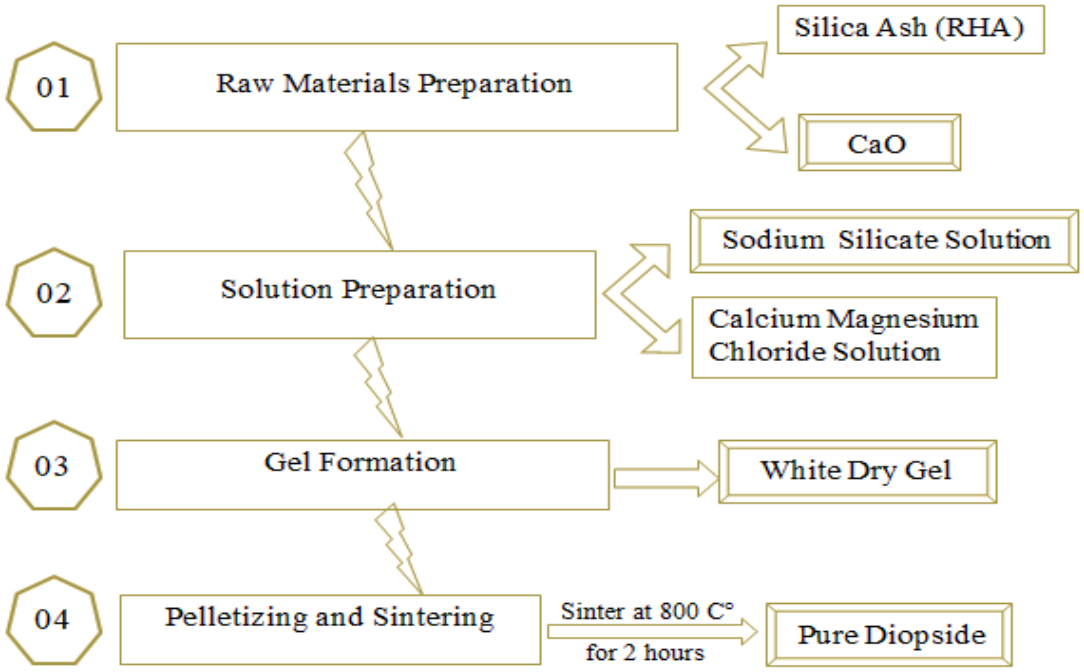


Fig. I.8. A diagram illustrating the experimental steps for preparing diopside using the sol-gel method.

➢ Characterization of diopside before and after soaking in SBF :

✓ X-ray diffraction :

The findings affirmed the presence of the monoclinic diopside phase ($CaMgSi_2O_6$), as evidenced by the XRD pattern **(Fig. I.9)** showing sharp and intense crystalline peaks. When immersed in simulated body fluid (SBF) over various durations-3, 7, 14, and 21 days-XRD analysis indicated a gradual dissolution of the diopside phase, which encouraged the development of hydroxyapatite. The first signs of hydroxyapatite peaks emerged after 7 days in immersion, with their intensity noticeably increasing at 14 and 21 days. The appearance of new diffraction peaks related to hydroxyapatite confirmed the material's capability to stimulate early-stage bioactivity by promoting hydroxyapatite deposition **[24].**

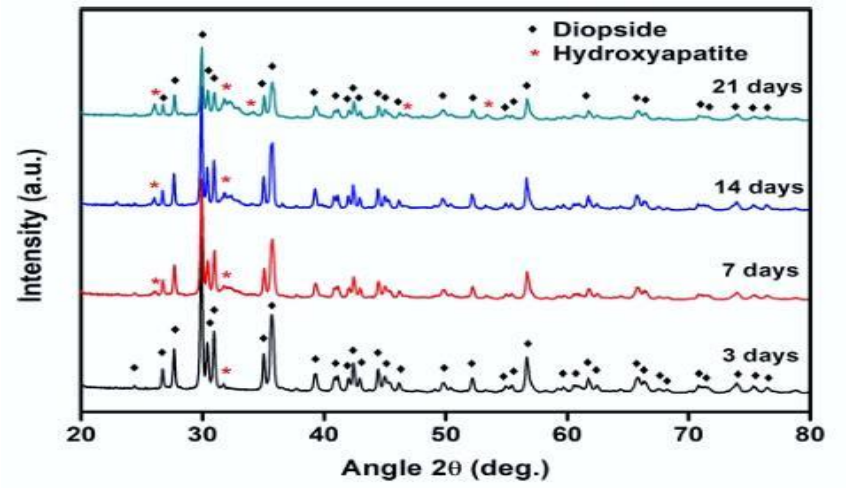


Fig. I.9. XRD patterns of diopside ceramics after immersion in SBF for 3, 7, 14 and 21 days.

✓ FTIR spectroscopy analysis :

The FTIR analysis of sintered diopside specimens identified all the characteristic functional groups typical of diopside **(Fig. I.10)**. These included non-bridging oxygen vibrations associated with calcium, magnesium, and silicon atoms, along with the stretching and bending modes linked to silicate structures. A moisture absorption band was also noted. After immersing the diopside samples in simulated body fluid for 14 days, changes in the FTIR spectra suggested the formation of hydroxyapatite on the surface. The silicate-related peaks decreased in intensity, while new phosphate-related peaks appeared, confirming the deposition of hydroxyapatite. Additionally, the presence of carbonate and water absorption bands indicated the formation of a carbonated hydroxyapatite layer, **Table. I.4** highlights the characteristic wavenumbers associated with these bonds **[24].**

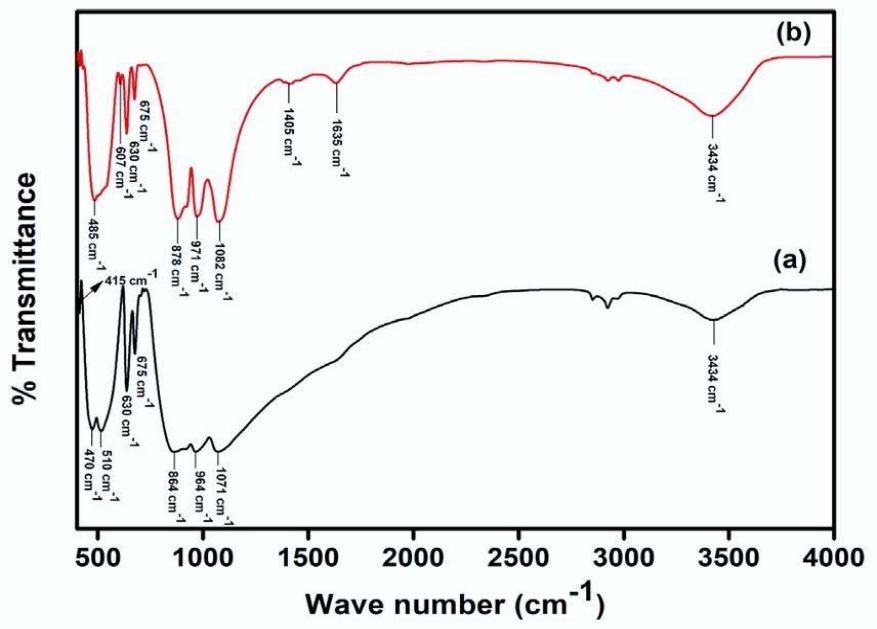


Fig. I.10. FTIR spectra of diopside ceramics (a) before and (b) after immersion in SBF for 14 days.

Table. I.4. Wavenumbers of FTIR spectra for diopside synthesized at 800°C.

	Absorption bands	Vibration mode	Wavenumbers	Ref
Before Soaking in SBF	O-Ca-O	Bending (NBO)	415 cm^{-1}	[24]
	O-Mg-O	Bending (NBO)	470 to 510 cm^{-1}	
	Si-O-Si	Bending	630, 675 cm^{-1}	
	Si-O	Stretching (NBO) Stretching (BO)	865 cm^{-1} 964, 1070 cm^{-1}	
	OH	Stretching	3434 cm^{-1}	
After soaking in the SBF	PO_4^{-3}	Bending Sym Stretching Asym Stretching	485 and 607 cm^{-1} 964 cm^{-1} 1082 cm^{-1}	
	CO_3^{-2}	Asym Stretching	1405 cm^{-1}	
	H_2O	Bending	1635 cm^{-1}	
	OH	Stretching	3434 cm^{-1}	

✓ **SEM analysis :**

The surface morphology of synthesized diopside ceramics, sintered at 800°C, was analyzed using SEM-EDS both before and after immersion in simulated body fluid (SBF) **(Fig. I.11)**. Prior to immersion, the surface displayed a porous nature with spherical particles ranging from 0.3 to 0.44 µm, a feature that aids in tissue interaction. EDS analysis confirmed the presence of essential elements such as calcium, magnesium, silicon, and oxygen, with no impurities detected, affirming the creation of pure diopside. After 14 days in SBF, leaf-like particles akin to hydroxyapatite began to form on the surface, increasing in abundance and distribution after 21 days. The EDS analysis showed a rise in phosphorus content over time, suggesting the material's ability to form hydroxyapatite and revealing its strong in vitro bioactivity **[24].**

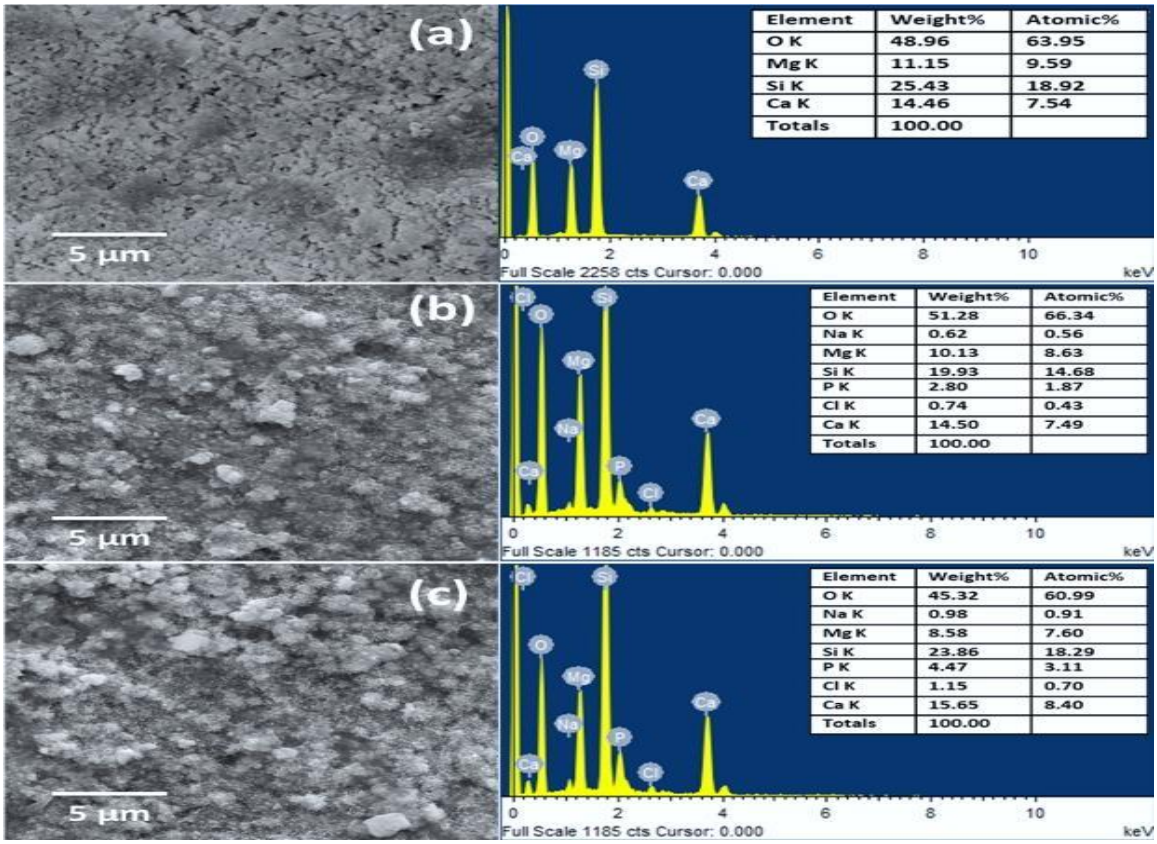


Fig. I.11. SEM-EDS of diopside ceramics (a) before (b) after 14 days and (c) after 21 days of immersion in SBF.

➢ Solid-State reaction :

The Solid-State Reaction method is a straightforward and cost-effective technique for synthesizing bioceramics. It involves the reaction of solid materials at elevated temperatures, making it a highly efficient approach.

✓ **Method :** The diagram **(Fig. I.12)** outlines the key experimental procedures for producing diopside through the solid-state reaction method, conducted at a sintering temperature of 1300°C **[25].**

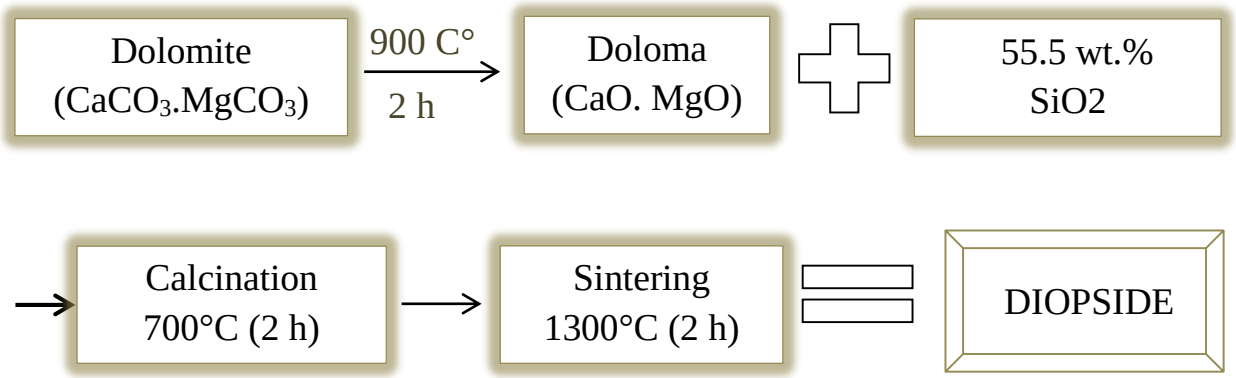


Fig. I.12. A diagram illustrating the experimental steps using the Solid-State Reaction method.

➢ Characterization of diopside before and after soaking in SBF:

✓ X-ray diffraction :

(A) before soaking in the SBF **(Fig. I.13a)** : XRD analysis verified the successful synthesis of pure monoclinic diopside ($CaMgSi_2O_6$). The lattice parameters measured were a = 9.776 Å, b = 8.979 Å, c = 5.267 Å, and β = 105.94°, corresponding with ICDD 01-072-1497. The crystallite size was approximately 660 nm, which is slightly larger than what is typically achieved through conventional methods. The vibratory milling technique yielded ultrafine diopside, free from impurities and without the need for acidic catalysts **[25].**

(B) after soaking in the SBF **(Fig. I.13b)** : X-ray diffraction analysis showed that diopside initially dissolved, leading to the formation of carbonated hydroxyapatite (CHA) after seven days, with notable peaks at 2θ values of 31.69° and 25.87°. The CHA continued to grow over the course of 21 days, increasing in crystallite size from 103 nm to 206 nm, while diopside retained predominance. This bioactive transformation points to promising applications in bone tissue engineering **[25].**

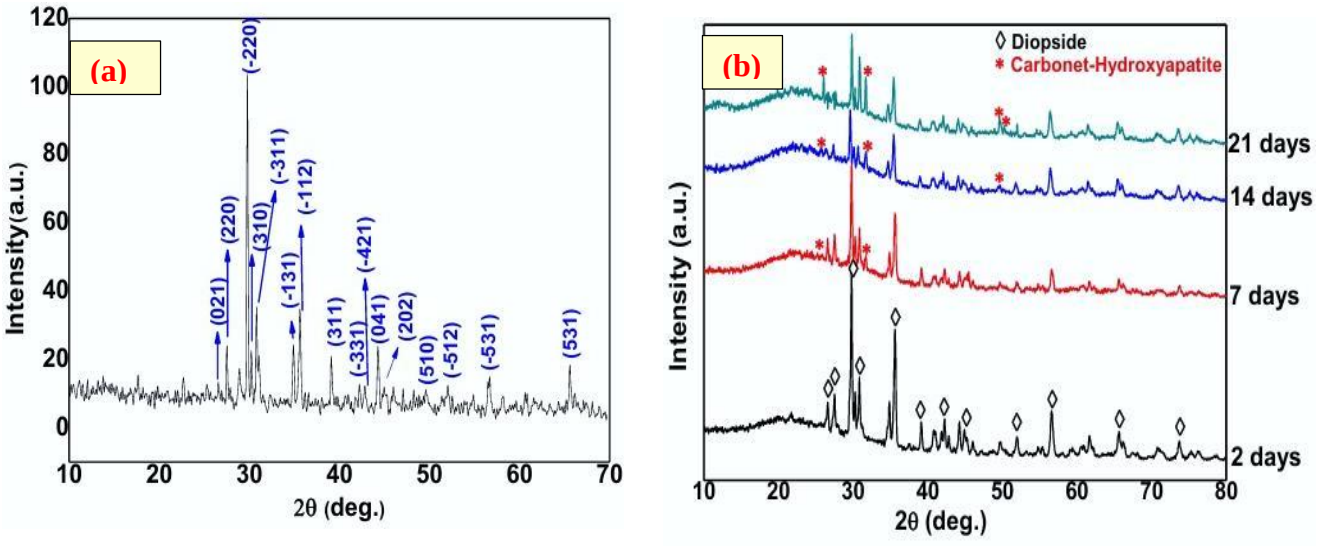


Fig. I.13. XRD pattern of diopside sintered at 1300 °C **(a)** before, **(b)** after soaking in the SBF.

✓ **FTIR spectroscopy analysis :**

FTIR analysis **(Fig. I.14)** verified the successful formation of diopside by revealing characteristic bonds between silicate and metal-oxygen. Upon immersion in simulated body fluid (SBF), there was a reduction in silicate bands, coupled with the emergence of phosphate and carbonate peaks. This suggests the formation of hydroxyapatite. Over time, the growth of carbonated hydroxyapatite (CHA) became apparent, further supported by vibrations related to phosphate and water. These results highlight diopside's bioactive potential for use in biomedical applications. **Table. I.5** shows the characteristic wavenumbers of the bonds **[25].**

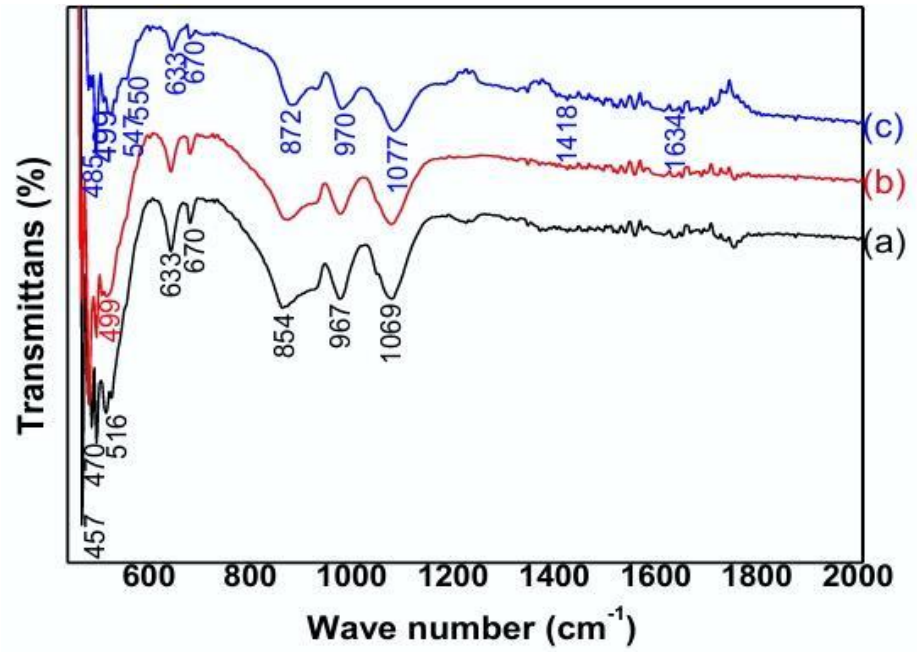


Fig. I.14. FTIR spectra of diopside powders **(a)** before, **(b)** after 2 days, and **(c)** after 21 days of immersion in SBF.

Table. I.5. Wavenumbers of FTIR spectra for diopside synthesized at 1300°C before and after soaking in the SBF.

	Absorption bands	Vibration mode	Wavenumbers (cm^{-1})	Ref
Before Soaking in SBF	O-Mg-O	Bending (NBO)	457 to 516 cm^{-1}	[25]
	O-Si-O	Bending	633 and 670 cm^{-1}	
	Si-O-Si	Sym Stretching	1069 cm^{-1}	
	Si-O	Sym Stretching	854 to 967 cm^{-1}	
After soaking in the SBF	PO_4^{-3}	–	499 cm^{-1}	
		Bending	485, 547 cm^{-1} 550 cm^{-1}	
		Stretching	972, 1077 cm^{-1}	
	CO_3^{-2}	–	1418 cm^{-1}	
	H_2O	Bending	1635 cm^{-1}	
	HPO_4^{-2}	Stretching	872 cm^{-1}	

✓ **SEM analysis :**

Figure I.15 illustrates the surface changes of ultrafine diopside granules after immersion in SBF for 2 and 21 days. After 2 days, small spherical particles and micropores (up to 7.41% area, ~5 µm size) appear, enhancing bioactivity. By 21 days, these pores disappear due to the formation of carbonated hydroxyapatite (CHA) crystals. This occurs through ion exchange, surface charge alteration, silica-rich layer formation, and subsequent calcium phosphate deposition, indicating bioactive behavior **[25]**.

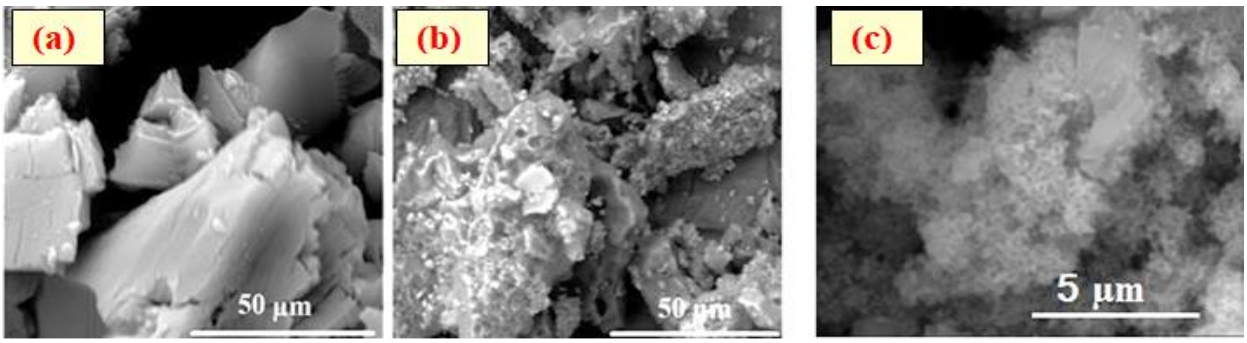


Fig. I.15. SEM images of the obtained diopside powders sintered at 1300 °C for 2 hours: **(a)** before, **(b)** after 2 days, and **(c)** after 21 days of immersion in SBF.

I.2.5. FTIR analysis of diopside before and after SBF Immersion: FTIR analysis of diopside before and after immersion in SBF using different synthesis methods was performed. FTIR analysis, conducted using these various methods, confirmed diopside formation and its bioactivity after SBF immersion. This is illustrated in the **Table. I.6.**

Table. I.6. FTIR Spectral Data of Diopside Samples Synthesized by Different Methods Before and After SBF Immersion.

	Absorption bands	Vibration mode	Wavenumbers (cm^{-1})	Ref
Before Soaking in SBF	O-Ca-O	Bending (NBO)	422	[26]
	O-Mg-O	Bending (NBO)	455 to 501	
	O-Ca-O	Bending (NBO)	420	[27]
	O-Mg-O	Bending (NBO)	455 to 503	
	O-Si-O	_	619, 648	
	Si-O-Si	_	1046	
	H_2O	Bending	1576	
	OH	Stretching	3445	
	CO_3^{-2}	Asym and Sym Stretching + Out of plane and in-plane Bending vibration	1450, 1050, 820 and 740	
	O-Ca-O	Bending (NBO)	412 to 422	[28]
	O-Si-O	Bending	632 and 675	
	Si-O-Si	Sym Stretching	1062	
	Si-O	Sym Stretching	997, 1093 854 and 960 (After calcination)	
	H_2O	Bending	1637	
	OH	_	3450	
After soaking in the SBF	PO_4^{-3}	Bending	480	[26]
		Stretching	972 and 1079	
	CO_3^{-2}	_	1405	
	H_2O	Bending	1697	
	OH	Moisture absorption	3385	

After soaking in the SBF	PO_4^{-3}	Bending	464, 509, 601	[28]
		Stretching	962, 1060	
	O-Si-O	Bending	634 (masked The OH functional group of apatite)	

I.2.6. Comparison between mechanical properties of diopside and human bone:

The mechanical properties of materials play a vital role in determining their suitability for biomedical applications. Human bone and diopside each possess unique mechanical characteristics, which makes comparing them particularly relevant when it comes to tissue engineering and implant design . **Table I.7** provides a comparison of their key mechanical properties.

Table. I.7. Comparison between mechanical properties of diopside and human bone.

Properties	Diopside (800°C)	Cortical bone	Cancellous bone	**Ref**
Microhardness (GPa)	7.31±0.1	0.322	0.30625	[24] [36]
Compressive strength (MPa)	210±12.5	100–230	2–12	
Fracture toughness ($MPam^{1/2}$)	2.8±0.3	2–12	_	
Bending strength (MPa)	86.7±7.3	50–150	_	
Elasticity modulus (GPa)	17.5±2.3	7–30	0.5–0.05	

I.2.6. Mechanism of interfacial bonding between bone tissue and diopside:

✓ Chemical stages :(Apatite formation on diopside surface in SBF) :

Before immersion, **Figure I.16a** depicts the ionic composition (such as Na^+, K^+, Cl^-, and Ca^{2+}) of a simulated body fluid. This setup includes a diopside sample prepared for immersion to analyze its interactions with the fluid, as referenced in studies **[29, 30].**

1. Dissolution: The release of calcium ions (Ca^{2+}) into the simulated body fluid (SBF) during the first day of immersion suggests the partial dissolution of pure diopside **[30]**. This process occurs due to an ion exchange mechanism involving calcium and magnesium ions (Ca^{2+}, Mg^{2+}) from the diopside interacting with hydronium ions (H_3O^+) in the surrounding SBF. This interaction is depicted in **Figure I.16b** and described by Equation **I.1**.

$$CaMg(SiO_3)_2 + 2H_2O \rightarrow Ca^{2+} + Mg^{2+} + 2HSiO_3^- + 2OH^- \quad \textbf{(I.1)}$$

2. Deposit and Growth: The progressive reduction in calcium ion concentration within the simulated body fluid highlights the initiation of apatite layer formation on the diopside sample surfaces, observed throughout the immersion period spanning days 1 to 11. This decrease can be attributed to the interaction between the perforated surface created by initial dissolution and the surrounding ions in the medium. The negatively charged diopside surface facilitates the attraction of positively charged calcium ions, encouraging the nucleation and gradual development of the apatite layer over time. **Figure I.16c** depicts this steady decline in calcium concentration, while **Figure I.16d** illustrates the complete apatite layer formation on the surface of the diopside samples.

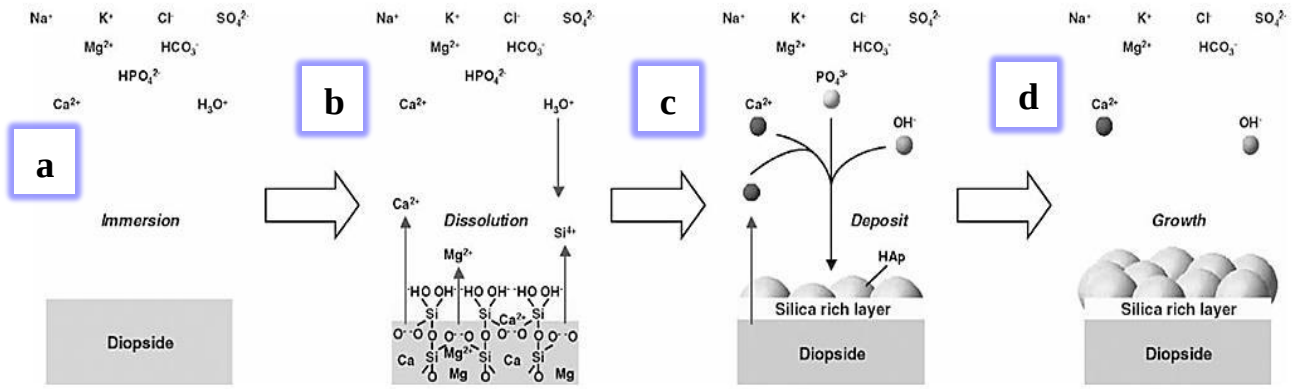


Fig. I.16. Schematic representation of the apatite-forming mechanism on the surface of Diopside in SBF.

✓ **<u>Biological response</u>:** The apatite layer formed on the surface of diopside activates stem cells, which initiates the biological response stages of bone tissue. **Figure I.17** illustrates these stages.

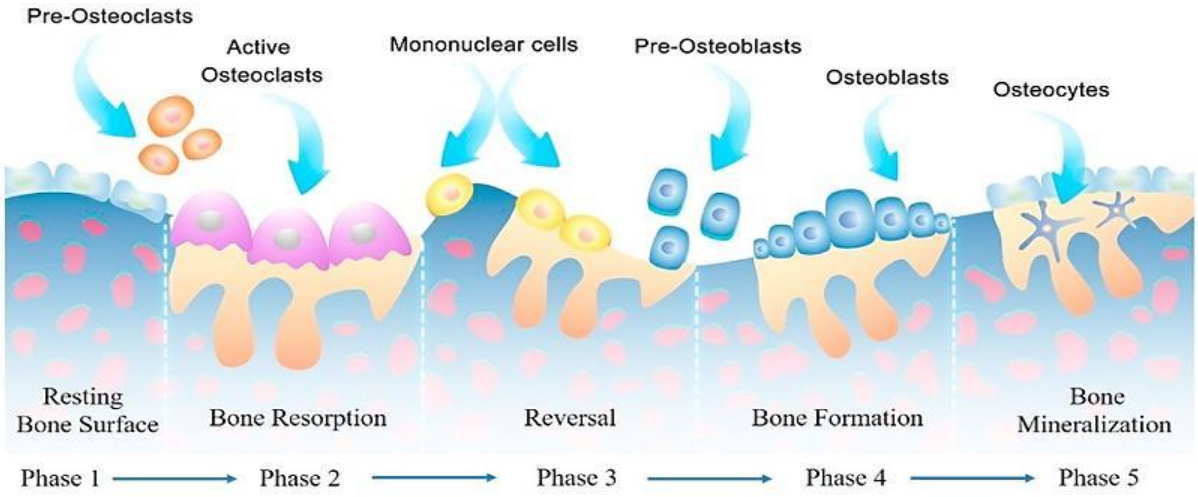


Fig. I.17. Schematic illustration of the normal bone remodeling process **[31].**

I .3. Overview of sintering :

I.3.1. Definition :

Sintering is a vital heat treatment process used in ceramics to transform powdered materials, shaped into a desired form, into solid bodies. This is achieved through atomic diffusion, whether in vapor, liquid, or solid phases, or through viscous flow in a glassy phase. Thermal activation helps overcome energy barriers, moving the material from a porous to a denser state. The process turns loose powder compacts, typically 40% porous and thus only 60% compact, into cohesive polycrystalline solids through particle bonding. By controlling microstructure components like grain size and porosity, sintering directly influences the material's performance. As a fundamental technique in ceramic processing, it facilitates consolidation while enhancing structural properties

[32,33,34].

I.3.2. Types of sintering process:

Sintering can be categorized into three main processes, driven by the material being fired and particularly the presence of a liquid phase during heat treatment:

1. Solid State Sintering: This process occurs entirely without any liquid phase. It involves only solid phases during sintering.

2. Liquid Phase Sintering: In this method, a small volume percentage of liquid phase is present at the sintering temperature.

3. Viscous Flow Sintering: This type of sintering features a high liquid phase volume, comparable to the porosity within the powder compact. Additionally, there is Reactive Sintering, where particle reactions lead to the formation of new product phases **[33,35].**

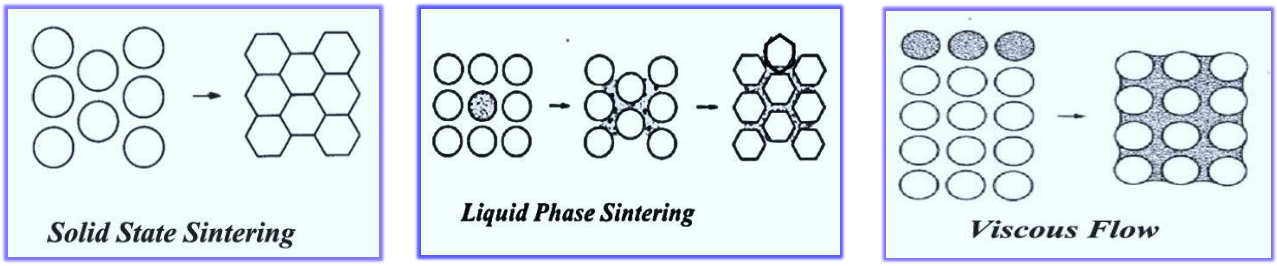


Fig. I.18. Types of sintering process **[33].**

I.3.3. Stages of Sintering:

The process of sintering unfolds in several distinct stages:

- **First Stage:** Initially, particles are simply in contact. As the temperature increases, additives begin to burn off, resulting in the formation and growth of necks at the points where particles touch.

- **Second Stage:** With enhanced atomic mobility, particle surfaces smooth out, and neck formation becomes more pronounced.

- **Third Stage:** Neck development continues, grain boundaries emerge, and material densification intensifies, significantly reducing porosity.

- **Fourth Stage:** This phase involves grain growth and the closure of pores, leading to the creation of isolated spherical bubbles **[33,35].**

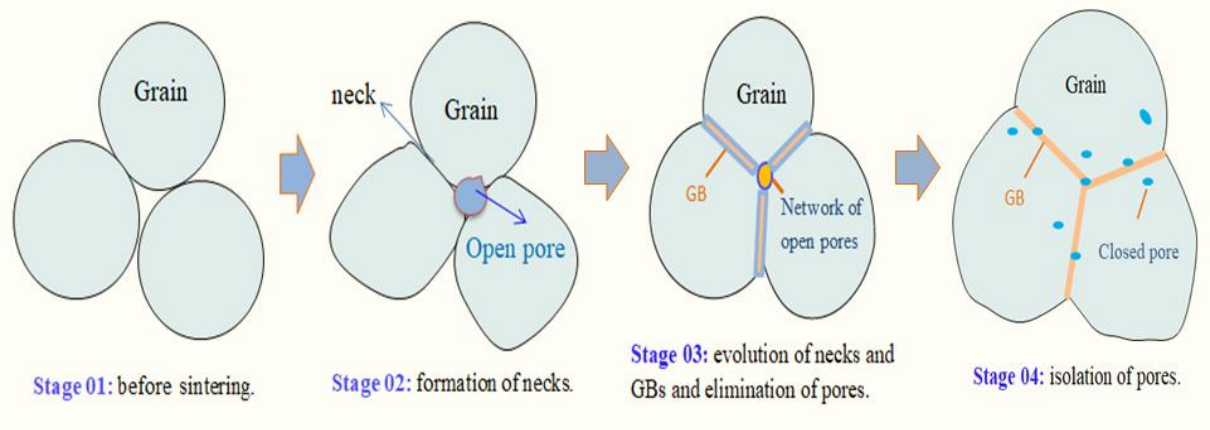


Fig. I.19. Different stages of sintering **[35].**



CHAPTER II

ELABORATION AND CHARACTERIZATION OF DIOPSIDE

II-Elaboration and Characterization of Diopside

This chapter outlines the experimental procedure for preparing pure diopside ($CaMgSi_2O_6$) and diopside doped with 0.5 wt.% sodium carbonate, utilizing the solid-state reaction method. The process primarily employs dolomite ($CaMg(CO_3)_2$) as a natural raw material, supplemented with laboratory-synthesized compounds. The prepared diopside samples are then immersed in Simulated Body Fluid (SBF) to assess the potential formation of an apatite layer on their surfaces under in vitro conditions. Characterization and analysis of the samples are conducted using X-ray diffraction (XRD) and Fourier-transform infrared spectroscopy (FTIR). The chapter concludes with a detailed description of the main equipment and techniques employed in the experimental work.

.

II .1. Experimental methods and materials :

✓ **Raw materials:**. Doloma (CaO.MgO) was produced using dolomite as the primary raw material, serving as a significant source of calcium and magnesium oxides. In addition, silicon oxide was utilized as a laboratory material. By carefully combining and processing these three oxides (CaO, MgO, SiO_2), diopside powder was successfully manufactured.

II .1.1. Overview of dolomite:

1. Definition : Dolomite ($CaMg(CO_3)_2$) is a sedimentary rock that primarily forms through the dolomitization of limestone, a process where calcite is replaced by dolomite in the presence of magnesium-rich solutions. It can also form directly through precipitation. Structurally, dolomite crystallizes in a rhombohedral unit cell **(refer to Fig. II.1)** with alternating layers of calcite ($CaCO_3$) and magnesite ($MgCO_3$). It is capable of forming solid solutions with elements such as iron, as illustrated in the phase diagram **(Fig. II.2),** which includes the formation of ankerite. Additionally, dolomite can incorporate trace elements like manganese, zinc, lead, strontium, cobalt, and nickel. Dolomite is found abundantly across the globe, is environmentally friendly, and is cost-effective to process. When pure, its magnesium oxide (MgO) content is about 40%. It is relatively soft, making it easy to grind into powder. In its pure form, dolomite appears colorless or pearly white, but impurities can give it shades of black, pink, brown, gray, or green **[37].**

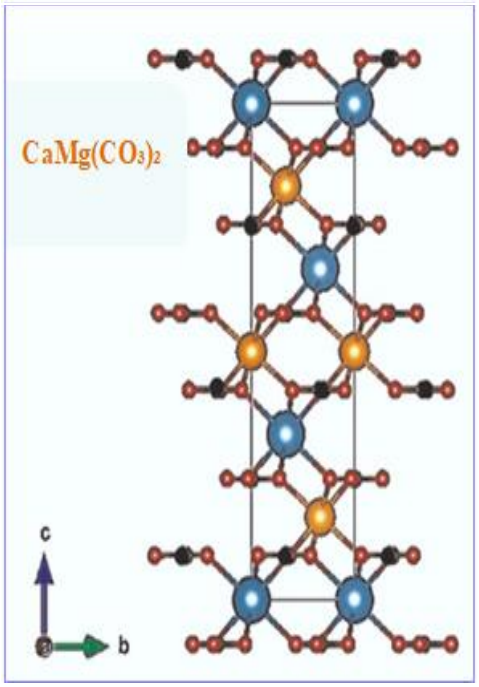


Fig.II.1. Crystal Structure of dolomite **[39].**

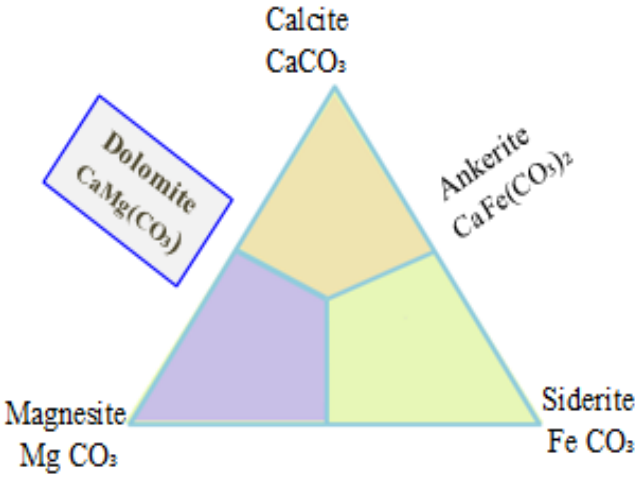


Fig.II.2. Ternary Phase Diagram of Carbonate Minerals ($CaCO_3$–$MgCO_3$–$FeCO_3$ System) **[38].**

2. The Key Properties of Dolomite: Every material possesses unique properties that distinguish it from others. **Table II.1** outlines the most significant characteristics of dolomite.

Table.II.1. Important Properties of Dolomite.

Properties		**Ref**
Name	Dolomite	**[37]**
Chemical Formula	$CaMg(CO_3)_2$ **or** $CaCO_3MgCO_3$	
Molecular weight	184.4	
Decomposition temperature (°C)	From 400	
brightness (%)	88-95	
Refractive index	1.6	

3. Characterisation of dolomite: This study focused on dolomite stone sourced from the Batna province in Algeria. Labeled as D1, this material features a light brown coloration and demonstrates a favorable density of 2.69 g/cm³, equating to 93.76% of the theoretical density for dolomite. The characterization process involved chemical analysis, differential thermal analysis (DTA), and infrared (IR) spectroscopy.

.

✓ **Chemical Analysis:** The chemical composition of the utilized dolomite rock sample was determined through X-ray fluorescence (XRF) analysis, as presented in **Table II.2** below. A reduction in sample weight was noted following the heating process.

Table.II.2. Chemical composition of the dolomite stone used **.**

Oxide	CaO	MgO	SiO_2	F_2O_3	Al_2O_3	Na_2O	SO_3	Weight loss
Weight (%)	30.41	21.86	0.00	0.27	0.07	0.02	0.46	46.91

✓ **Differential thermal analysis (DTA) results,** shown in **Fig. II.3**, depict the thermal behavior of the dolomite sample, highlighting two distinct endothermic peaks associated with the decomposition of its primary carbonate phases. The first peak, occurring at approximately 700°C, signifies the breakdown of calcium carbonate ($CaCO_3$) and the release of carbon dioxide (CO_2). The second peak, detected near 900°C, corresponds to the decomposition of magnesium carbonate ($MgCO_3$), which is also accompanied by the release of CO_2. These thermal events culminate in the formation of doloma, a mixed oxide consisting of calcium and magnesium oxides.

.

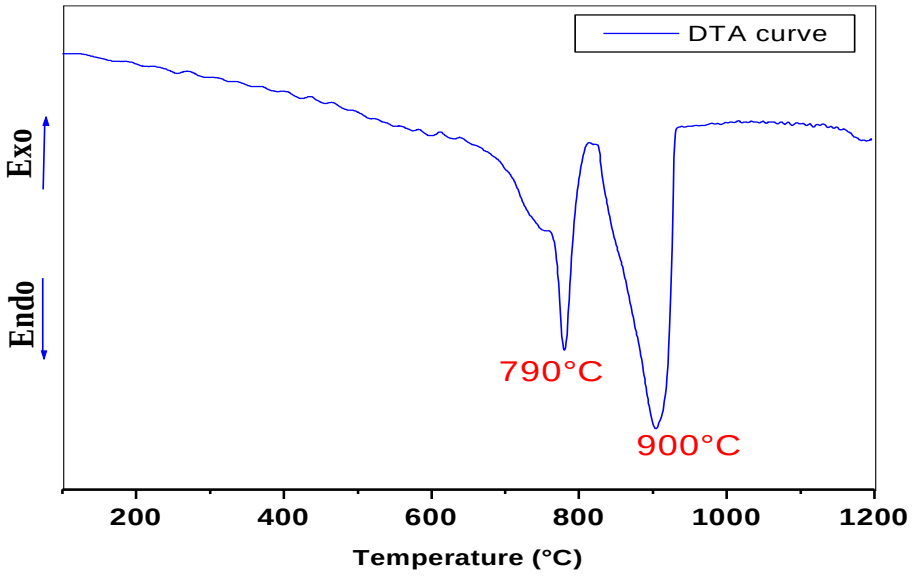


Fig.II.3. DTA curve of a local dolomite stone sample.

✓ **Fourier Transforms Infrared Analysis (FTIR):**

Figure II.4 illustrates the infrared transmission spectrum of a natural dolomite sample, highlighting key spectral features associated with its composition. The spectrum displays distinct absorption peaks characteristic of the carbonate group (CO_3^{2-}). Two prominent peaks appear at 726 cm^{-1} and 878 cm^{-1}, corresponding to the in-plane bending (ν_4) and out-of-plane bending (ν_2) vibrational modes, respectively. Moreover, a peak at 1441 cm^{-1} is attributed to the asymmetric stretching vibration (ν_3).

In addition, two combination bands were identified at 1869 cm^{-1} and 2526 cm^{-1}, associated with complex vibrational modes within the carbonate group, specifically ($\nu_1 + \nu_4$) and ($2\nu_2 + \nu_4$), respectively **[40.41]**. These reflect the intricate vibrational interactions inherent in natural dolomite's structure.

An absorption band observed at 1031 cm^{-1} does not align with typical carbonate vibrations. This feature is likely linked to the structural characteristics of the dolomite sample itself, such as variations in its crystal lattice or impurities influencing the spectral profile.

Overall, the analysis confirms that the sample consists of natural dolomite, as evidenced by its characteristic carbonate spectra, while also exhibiting additional spectral features potentially related to its unique structural and compositional attributes.

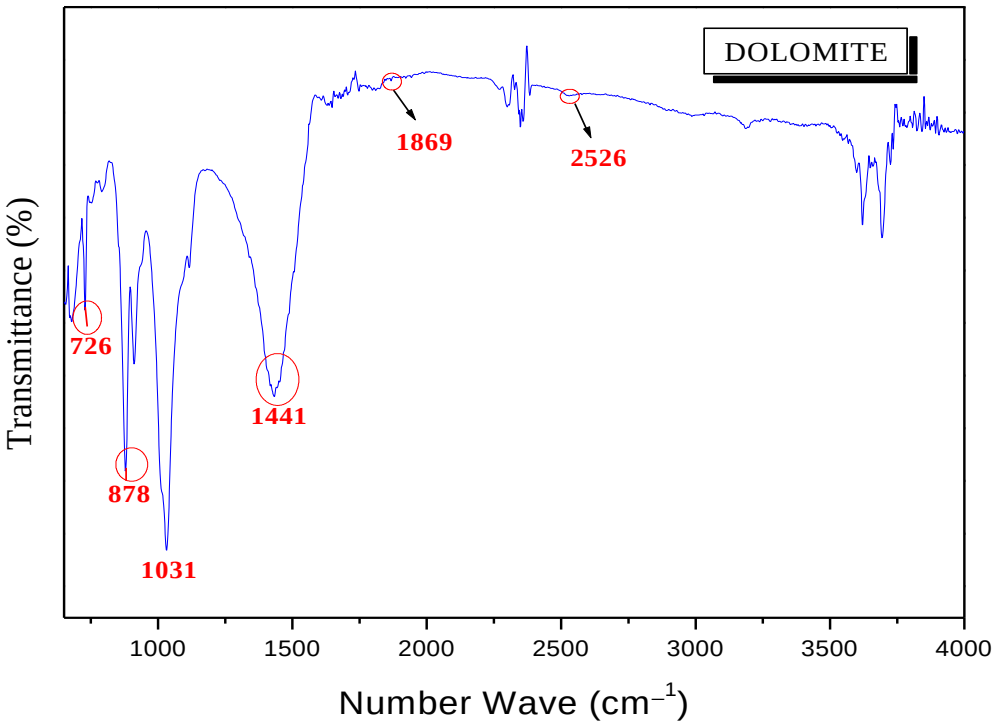


Fig.II.4. FTIR analysis of natural dolomite.

Table.II.3. Vibrational frequency assignments (FT–IR).

Vibration mode	ν_2 (cm^{-1})	ν_3 (cm^{-1})	ν_4 (cm^{-1})	$\nu_1 + \nu_4$ (cm^{-1})	$2\nu_2 + \nu_4$ (cm^{-1})
CO_3^{-2}	878	1441	726	1869	2526

II .1.2. Silicon oxide SiO_2 :

1. Definition: Silica is an essential constituent of the Earth's crust, found in both crystalline **(see Fig. II.5)** and amorphous **(see Fig. II.6)** forms. Within soils, it is primarily present in crystalline structures such as quartz, tridymite, and cristobalite. However, for the purposes of our experiment, the focus will be on the amorphous phase of silica **[42.43]**.

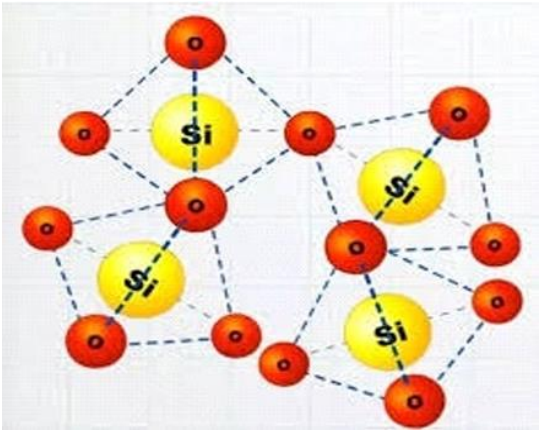


Fig.II.5. Crystal Structure of SiO_2.

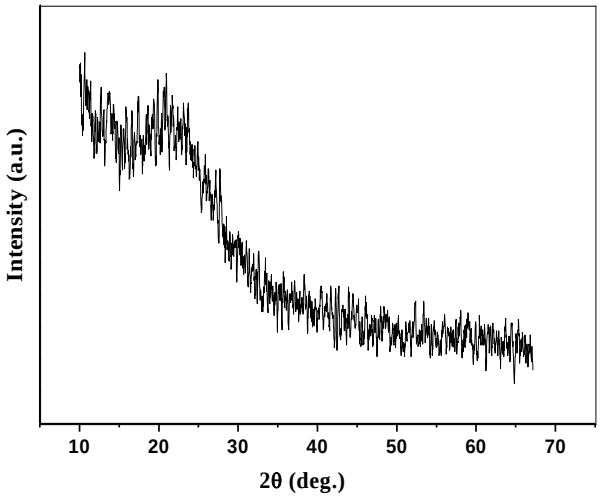


Fig.II.6. Amorphous Structure of SiO_2.

2. The Key Properties of SiO_2: Every substance is characterized by unique physical and chemical properties. **Table II.4** highlights the primary features of silicon dioxide (silica).

Table.II.4. Important Properties of SiO2 (Silicon dioxide).

Properties		**Ref**
Name	Silicon oxide	**[42]**
Chemical Formula	SiO_2	
Crystal structure	Amorphous	
Melting point (°C)	1700	
Density (g/cm^3)	2.27/2.18	
Atomic weight (g/mole)	60.08	

II .1.3. Addition: Sodium carbonate Na_2CO_3 :

1. Definition:

Sodium carbonate, commonly known as soda ash, is a white, crystalline, hygroscopic powder with a purity exceeding 99.5% when calculated in its anhydrous form. It is available in two variants: light soda and dense soda. Sodium carbonate crystallizes in the monoclinic system **(refer to Fig. II.7)**. Potential impurities in sodium carbonate include sodium chloride, sodium sulfate, calcium carbonate, magnesium carbonate, sodium bicarbonate, and iron. The impurity profile varies depending on the production method and the composition of the raw materials used **[44]**.

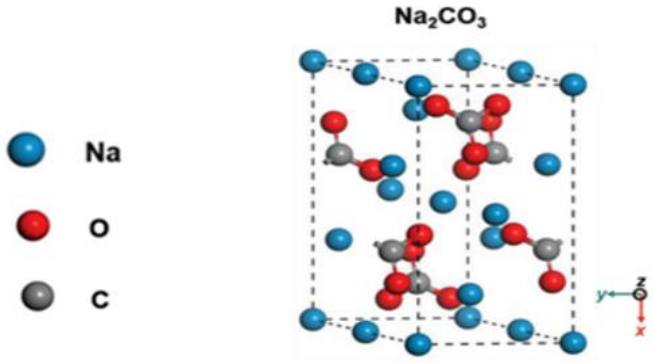


Fig.II.7. Crystal Structure of Na_2CO_3 **[48].**

2. The Key Properties of Sodium Carbonate: Every material possesses unique properties that distinguish it from others. **Table II.5** outlines the most significant characteristics of sodium carbonate.

Table. II.5. Important Properties of Na_2CO_3 (**S**odium carbonate).

Properties		**Ref**
Name	**S**odium carbonate	**[44]**
Chemical Formula	Na_2CO_3	
Synonyms	Soda ash; Calcined soda; Carbonic acid disodium salt	
Melting Point (°C)	851	
Density (20 °C) (g/cm^3)	2.532	
Particle size (µm)	Light sodium carbonate: 90 – 120 Dense sodium carbonate: 250 – 400	

II .1.4. preparation of specimens:

1. preparation of doloma:

Diopside ceramics were synthesized using a solid-state reaction method, employing high-purity raw materials sourced locally, specifically dolomite. Doloma, composed of CaO and MgO, was prepared by calcining Algerian dolomite ($CaCO_3 \cdot MgCO_3$) in an oven at 900°C for 2 hours. The X-ray diffraction analysis of the raw dolomite is depicted in **Fig. II.8.A**, while **Fig. II.8.1** displays the XRD pattern post-calcination. This thermal decomposition results in the complete release of CO_2, a fact verified by differential thermal analysis, and produces a white, friable solid that easily disintegrates into fine powder with minimal mechanical pressure. XRD analysis of this powder, seen in **Fig. II.8.2**, confirms the successful formation of doloma.

To improve the sintering behavior, the doloma underwent a hydration treatment to modify the grain morphology by converting CaO and MgO into their hydroxides -$Ca(OH)_2$ and $Mg(OH)_2$-. A ratio of 50 mL of distilled water was used per 20 g of doloma. While CaO reacts exothermically with water at ambient temperature, transforming MgO necessitated heating at 150°C in a drying oven. This resulting sample is referred to as highly hydrated doloma. Subsequent calcination at 600°C for 2 hours led to the decomposition of the hydroxides - $Mg(OH)_2$ at approximately 350°C and $Ca(OH)_2$ around 580°C - reverting them to oxides within a restructured microstructure conducive to sintering. XRD analysis of the calcined material confirmed the formation of restructured doloma, as shown in **Fig. II.8.3**. The detailed steps of the experimental procedure are illustrated in **Fig. II.9**.

2. preparation of diopside:

To prepare diopside ($CaMgSi_2O_6$), a carefully measured blend was created by mixing the second calcined doloma (containing 58.18 wt.% CaO and 41.82 wt.% MgO) with 55.49 wt.% high-purity silica (SiO_2, 99.9 wt.%). This mixture underwent wet milling in a cylindrical chamber, utilizing zirconia balls and roughly 200 mL of distilled water per 20 g of solid. After 4 hours of milling, the resulting slurry was dried at around 150°C and then calcined at 700°C for 2 hours to initiate the creation of an amorphous precursor. XRD analysis **(Fig. II.10)** showed the milled and calcined powder to be largely amorphous, with no discernible crystalline peaks, suggesting mechanical milling and thermal treatment disrupted its long-range order.

Part of the produced diopside powder was pressed uniaxially at 112 MPa into disk-shaped pellets measuring 13 mm in diameter and sintered without any additives. To improve sinter ability, 0.5 wt.% sodium carbonate (Na_2CO_3) was introduced as a sintering aid. The modified powder then underwent a second grinding session for 15 minutes followed by another calcination at 700°C for 2 hours to integrate the additive properly and adjust its structure. These powder samples were again pressed uniaxially at 112 MPa into disk-shaped pellets with a diameter of 13 mm.

Finally, the samples were sintered at 1250°C for 2 hours. The detailed steps of this experimental procedure are illustrated in **Fig. II.11**.

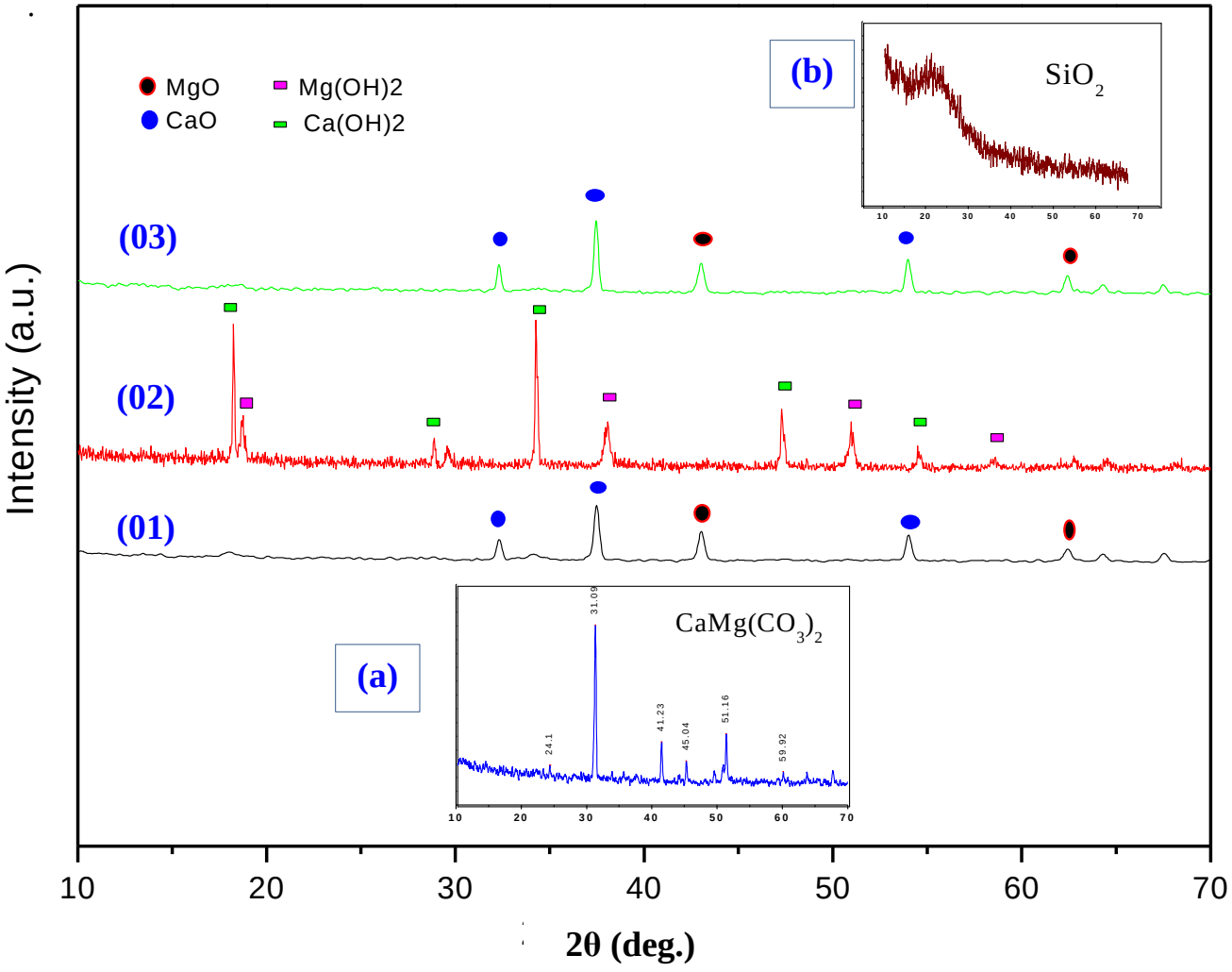


Fig.II.8. (XRD) patterns of **(a)** raw dolomite **(01)** dolomite cal (doloma) **(02)** doloma hyd **(03)** doloma hyd cal **(b)** silicon oxide.

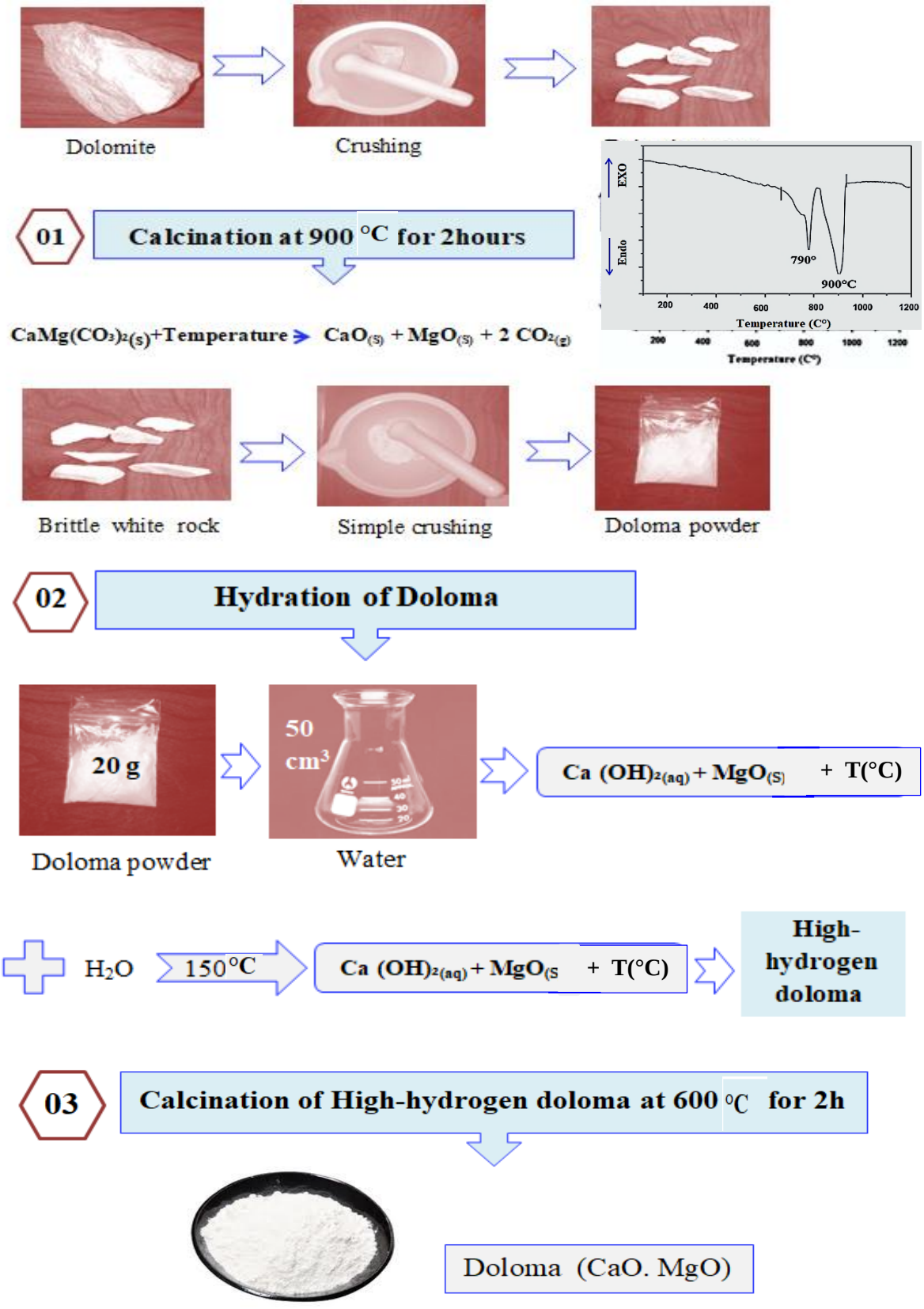


Fig.II.9. Experimental Procedure for Preparing doloma.

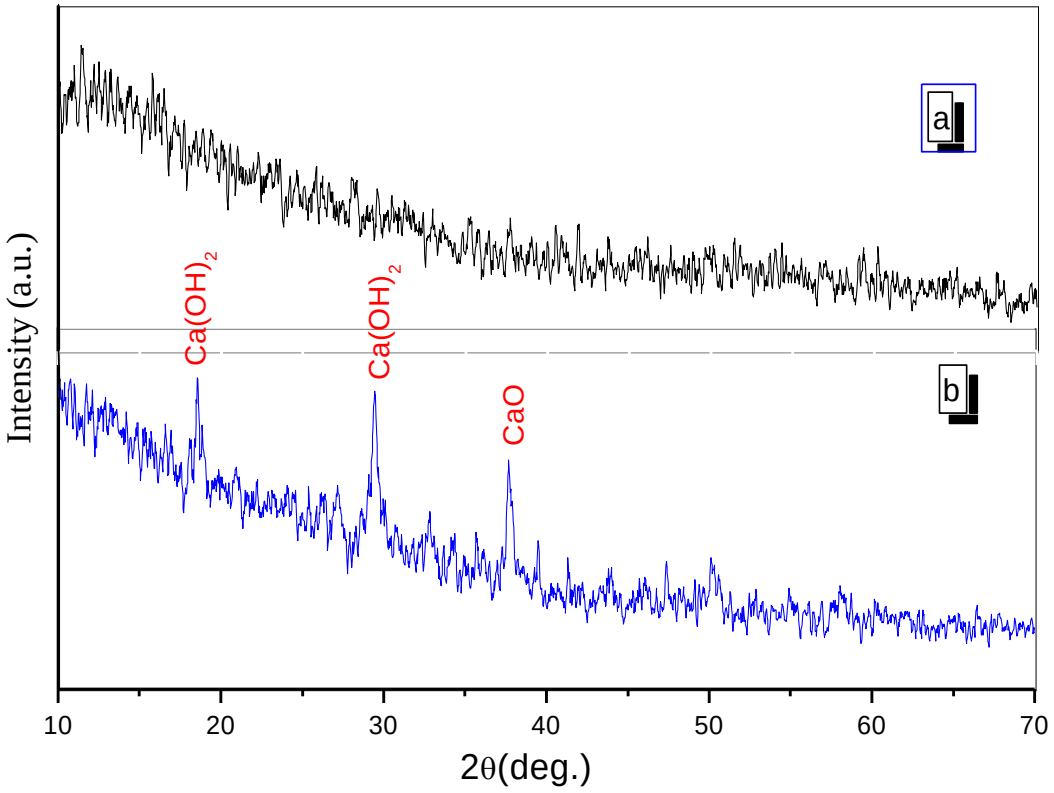


Fig.II.10. (XRD) patterns of **(a)** after grinding and **(b)** after grinding followed by calcination.

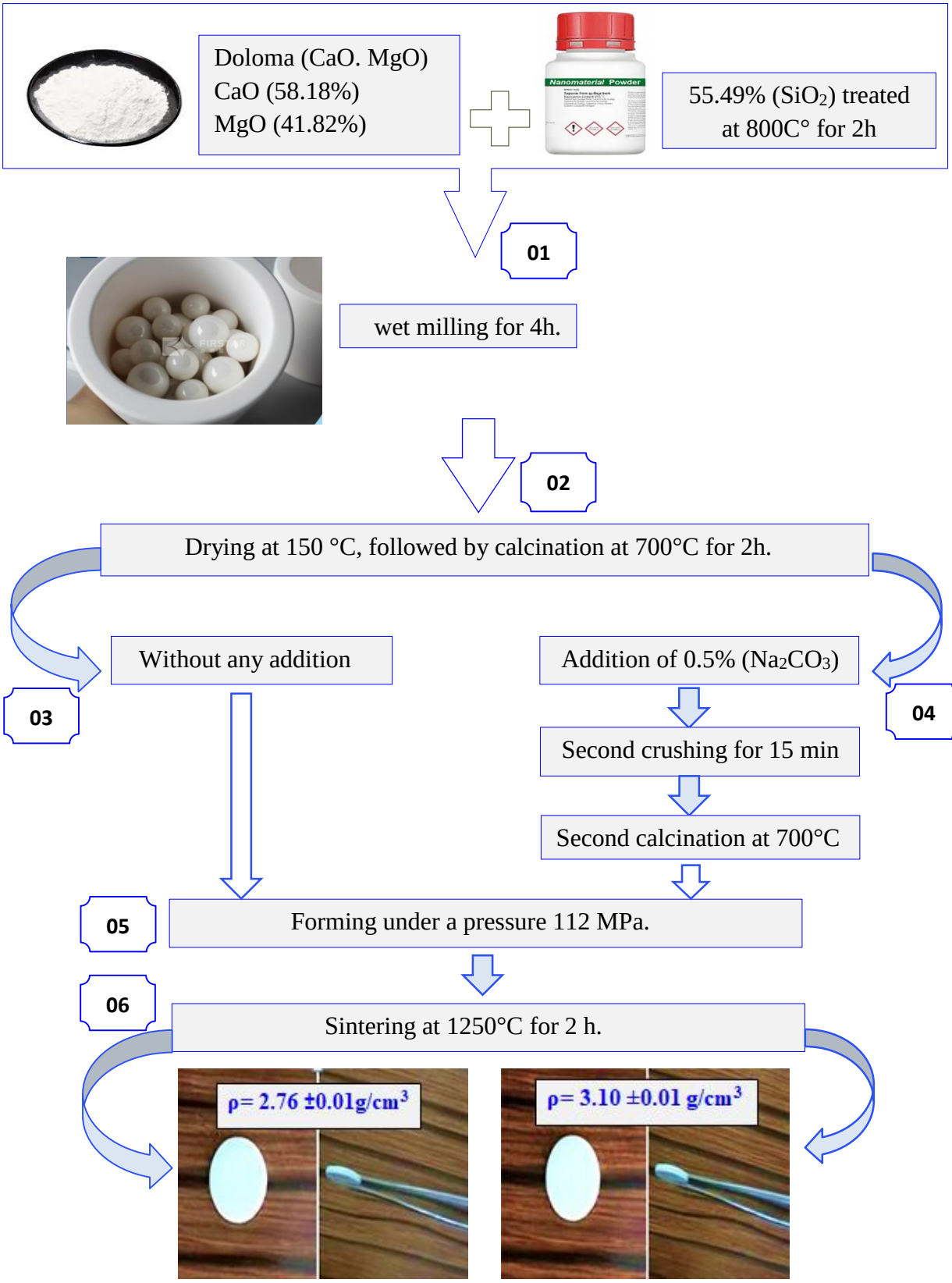


Fig.II.11. Experimental Procedure for Preparing diopside samples.

3. In Vitro Bioactivity Analysis :

✓ Preparation of simulated body fluid (SBF) :

The simulated body fluid (SBF) utilized in this study was prepared following the protocol designed by Kokubo and Takadama **[25]**, which mimics the ionic composition of human blood plasma, as outlined in **Table II.5**. Reagent-grade chemicals listed in **Table II.6** were dissolved in distilled water under constant magnetic stirring. Specifically, the appropriate amounts of NaCl, KCl, $CaCl_2$, $MgCl_2 \cdot 6H_2O$, $K_2HPO_4 \cdot 3H_2O$, and $NaHCO_3$ were gradually added to 750 mL of distilled water in a glass volumetric flask. After all components were fully dissolved, the solution's temperature was adjusted to 37 °C using a hot-stirrer to replicate physiological conditions.

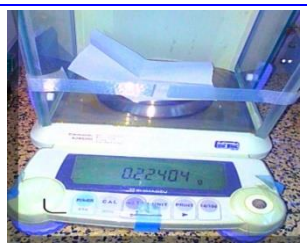
The pH of the solution was meticulously adjusted to 7.4 by slowly adding 1M hydrochloric acid (HCl) to match the physiological pH of human plasma. Finally, the solution's volume was increased to 1000 mL with distilled water. **Figure II.12** provides a detailed overview of the experimental procedure.

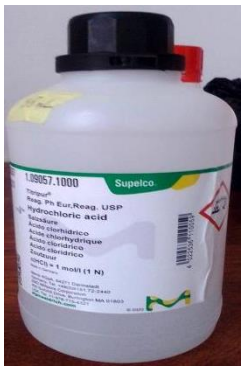
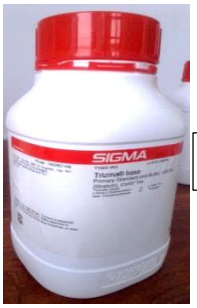
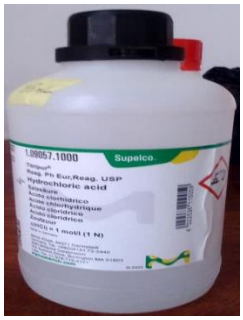
.

Table.II.6. Ion concentration in SBF and human blood plasma **[25].**

Ion	Ion concentration (mmol/L)	
	SBF	Blood plasma
Na^+	142.0	142.0
K^+	5.0	5.0
Mg^{2+}	1.5	1.5
Ca^{2+}	2.5	2.5
Cl^-	147.8	103.0
HCO_3^-	4.2	27.0
HPO_4^{2-}	1.0	1.0
SO_4^{2-}	0.5	0.5

Table.II.7. Components required for the preparation of simulated body fluid (SBF).

Order	Chemicals	Amount (for100mL of solution)
01	 NaCl	 7.996g
02	 $NaHCO_3$	 0.350g
03	 KCl	 0.224g
04	 $K_2HPO_4.3H_2O$	 0.227g
05	 $MgCl_2.6H_2O$	0.305 g

06	 Solution 1N-HCl	 35ml
07	 $CaCl_2.H_2O$	 0.368g
08	 Na_2SO_4	 0.071g
09	 $(CH_2OH)_3CNH_2$	 6.057g
10	 1N-HCl	 10 ml

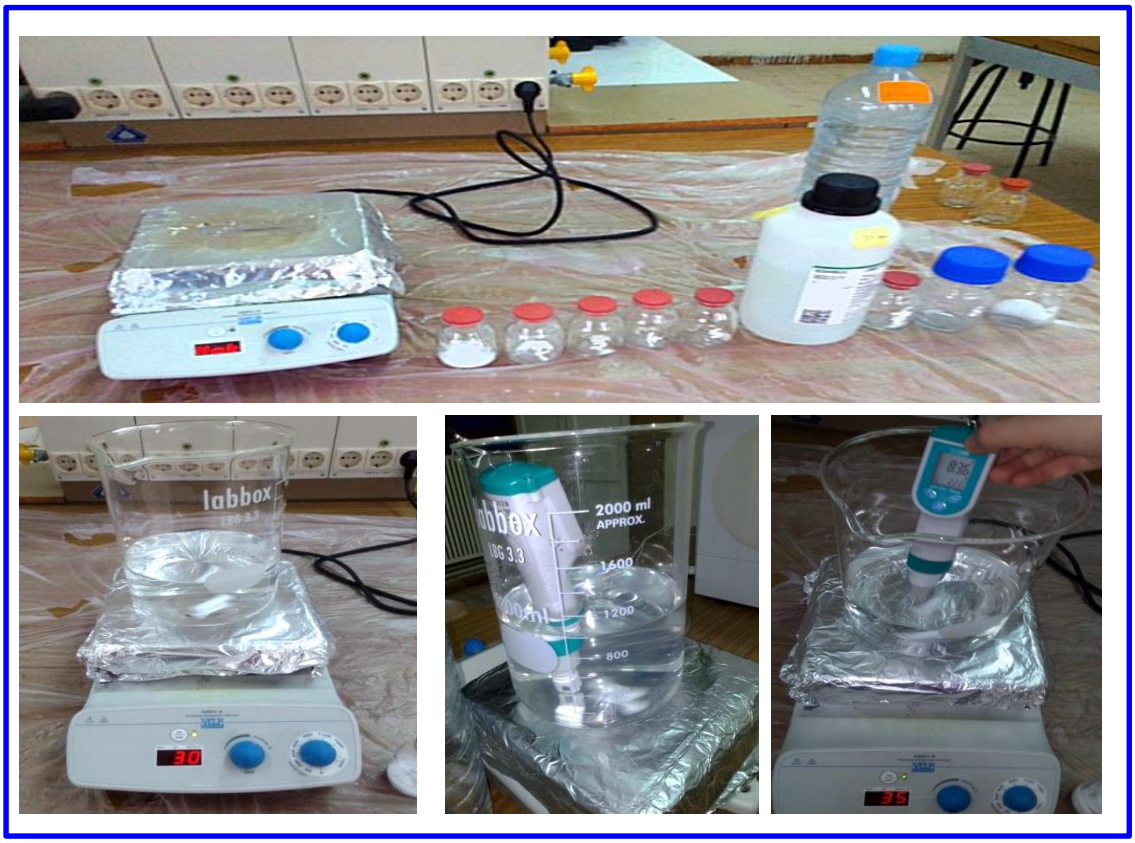


Fig.II.12. Experimental Procedure for Preparing SBF.

✓ Immersion of the samples in simulated body fluid (SBF):

After sintering at 1250 °C for 2 hours, the pure diopside samples and those containing 0.5 wt.% Na2CO3 were milled to obtain powders. The in vitro test began with weighing the diopside samples both before and after the inclusion of Na2CO3. Each sample of powder was then weighed **(see Fig. II.13)** and divided into six equal portions, making a total of 12 sub-samples. Of these, ten were designated for immersion in simulated body fluid, while the remaining two served as unsoaked controls.

The soaking process involved immersing 10 mg of each powdered sub-sample in 100 mL of SBF at 37 °C for various durations: 4 hours, and 1, 4, 7, and 11 days. A commercially available egg incubator was used to maintain a stable temperature and provide gentle agitation, consistently heating the samples at 37 °C with mild vibration. After each immersion period, the samples were separated from the solution, and then the samples were gently rinsed with 10 mL of distilled water for 5 minutes before being air-dried **(refer to Fig. II.14)**.

The bioactivity of the samples was evaluated by examining their ability to form apatite in the SBF.

.

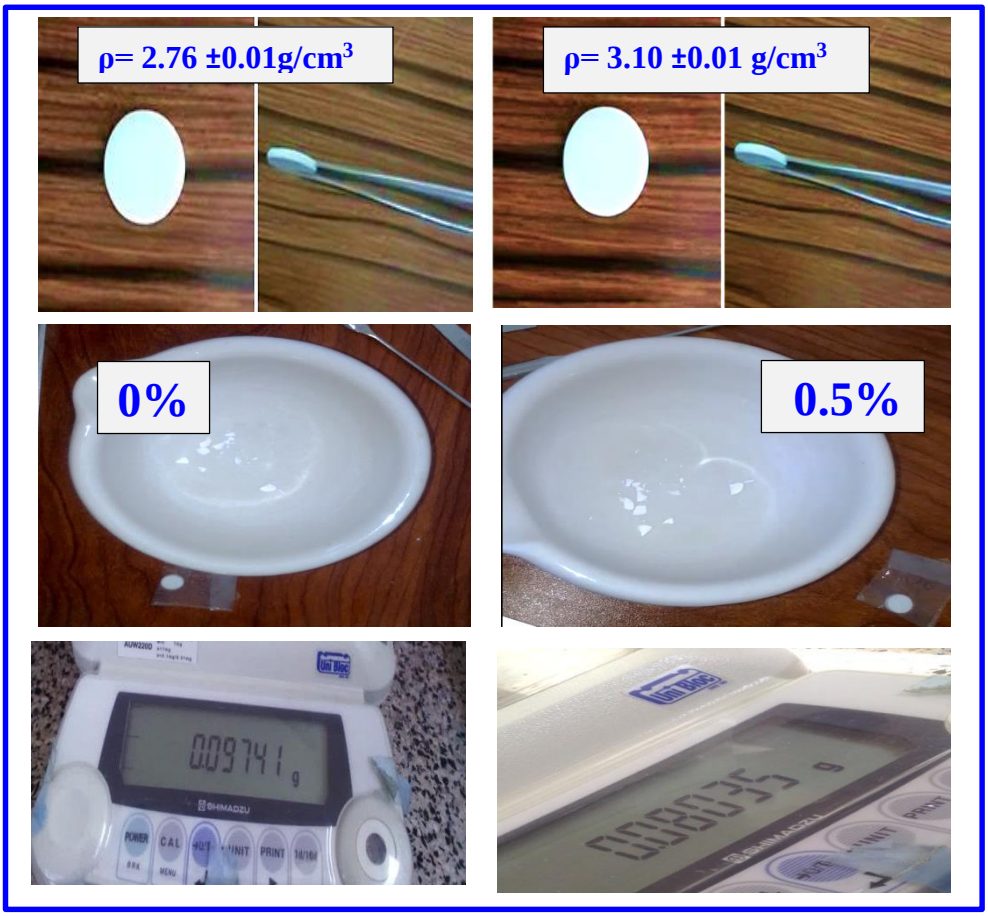


Fig.II.13. Preparation and Weighing of Crushed Diopside Samples.
(The weight here is divided by 6).



Fig.II.14. Diopside samples after immersion in SBF and subsequent drying.

II.2. Characterisation Techniques and Equipments:

II.2.1. Characterisation Techniques:

Fourier Transform Infrared spectroscopy was utilized to evaluate the bioactivity of diopside before and after the addition of 0.5% sodium carbonate, providing insights into its molecular structure. Differential Thermal Analysis was carried out to study the thermal behavior and phase transformations, covering a temperature range of 30–1200°C. X-ray Diffraction was employed for accurate phase identification. The elements and phases identified during the study were analyzed with the HighScore Plus software linked to X-ray diffraction data. Crystallite size was calculated using the Scherrer formula :

$$D = \frac{0.90\lambda}{FWHM\cos\theta} \quad \text{..... (II- 1)}$$

In this context: λ represents the X-ray wavelength, which is 1.54056 Å; θ denotes the Bragg diffraction angle of the XRD peak; and FWHM stands for the full width at half maximum.

II.2. Equipments:

In any scientific experiment, the instruments and equipments are vital for ensuring accurate results and safe procedures. These tools allow for precise operations, measuring variables, and controlling experimental conditions. In this experiment, a variety of scientific instruments were employed, each contributing significantly to achieving the study's goals. The following sections will outline the most important of these devices and their essential functions within the experimental framework.

II.2.2.1. Crushing device (Mortar and Pestle) :

The manual crushing tool, depicted by the mortar in **Figure II.15**, was initially utilized for breaking down dolomite rock samples, Subsequently, it was also used to crush sintered diopside.



Fig II.15. Crushing device.

II.2.2.2. Balance:

A precision balance of the SHIMADZU AUW 220D type, as illustrated in **Fig II.16**, was utilized. It offers a measurement accuracy of Δm = 0.01 mg.



Fig II.16. A precision balance of the " SHIMADZU AUW 220D" type.

II.2.2.3. Incubator :

A specialized incubator was employed as an alternative to the original device. The Egg Incubator 96 Eggs model **(Fig II.17)** is fully automatic, offering precise temperature control from 30°C to 39°C, along with a humidity regulation system. It features an automatic vibration or rotation mechanism to ensure even heat distribution. The device includes a digital display showing temperature, humidity, and operating time, and functions on a 110–240V power supply with a power rating of 100W. In this study, the incubator was used for immersing diopside powder in SBF solution at various time intervals.



Fig II.17. Automatic incubator type " Egg Incubator 96 Eggs ".

II.2.2.4. Magnetic heater :

To mix and homogenize different chemical solutions and compounds for the preparation of SBF at a specific temperature, we used a heater equipped with magnetic stirring **(Fig II.18)**.



Fig II.18. Magnetic heater.

II.2.2.5. pH Meter:

To measure the pH level of the solutions, we used the Waterproof Pen Tester pH/mV/Temp device, which is capable of measuring both temperature and the pH of the solution **(Fig II.19)**.



Fig II.19. pH Meter.

II.2.2.6. FTIR spectroscopy:

In this study, we utilized the JASCO FT/IR-4X Fourier Transform Infrared Spectrometer. This high-performance Mid-IR instrument (range: 7800–350 cm^{-1}) is designed for precise identification of chemical bonds and functional groups. It includes a temperature-controlled DLaTGS detector, ceramic IR source, and ATR-PRO 4X accessory with options for diamond, Ge, or ZnSe prisms, making it suitable for both routine and advanced spectroscopic analysis (**Fig II.20)**.



Fig II.20. FT/IR-4X Fourier Transform Infrared (FTIR) Spectrometer.

II.2.2.8. XRD spectroscopy:

The Bruker D8 ADVANCE is a sophisticated X-ray diffraction system produced by Bruker in Germany, designed for examining the crystalline structure of solid materials. This system allows for the identification of crystal phases, measurement of crystallite size, and analysis of structural changes with high precision. It is commonly used in the evaluation of metals, ceramics, polymers, and thin films. In this study, we utilized a D8 ADVANCE model **(referenced in Fig II.21)** to analyze the crystalline structure of the sample and determine the nature of its constituent phases.



Fig II.21. XRD spectrometer.

II.2.2.9. Electric oven:

In our experiment, we utilized a NABERTHERM furnace, which offers high precision in temperature control. This enables accurate and efficient execution of thermal processes **(Fig II.22).**

.



Fig II.22. Electric oven type " NABERTHERM ".

II.2.2.10. Mechanical compactor:

A mechanical compressor of the Specac type is utilized, as shown in **Figure II.23**.

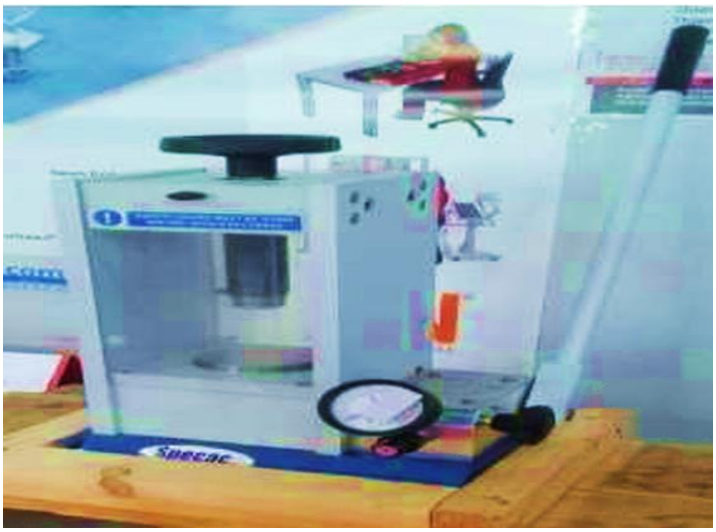


Fig II.23. A mechanical compactor of the Specac type.



CHAPTER III

RESULTS AND DISCUSSION

III-Results and discussion

Chapter Three presents the experimental results and their analysis in relation to previous studies. In this study, bioactive diopside ($CaMgSi_2O_6$) was synthesized through sintering at 1250°C for 2 hours. The chapter investigates the impact of adding 0.5 wt.% sodium carbonate (Na_2CO_3) on the crystallization and sintering behavior of diopside. Additionally, it explores how this addition affects the bioactivity of the sintered diopside and assesses the formation of an apatite layer following immersion in SBF.

III-1 Structural properties before immersion in simulated body fluid (SBF):

III-1-1 Investigating the impact of adding 0.5 wt.% Na_2CO_3 on the crystallization:

In this study, diopside compound ($CaMgSi_2O_6$) was doped with 0.5% by weight of sodium carbonate (Na_2CO_3) using the solid-state reaction method. The effect of this addition on the crystallization of samples treated at a temperature of 740°C was examined using X-ray diffraction (XRD) with a Cu Kα monochromatic radiation source (λ = 1.54056 Å), in line with the study's objectives. The differential thermal analysis (DTA) results indicate that diopside crystallization begins at approximately 750°C **(Fig.III.1)**. This explains the absence of diffraction peaks corresponding to diopside in untreated samples processed at 740°C. However, diopside can be crystallized at this temperature with the addition of 0.5% sodium carbonate, as illustrated in the fig.III.2 provided.

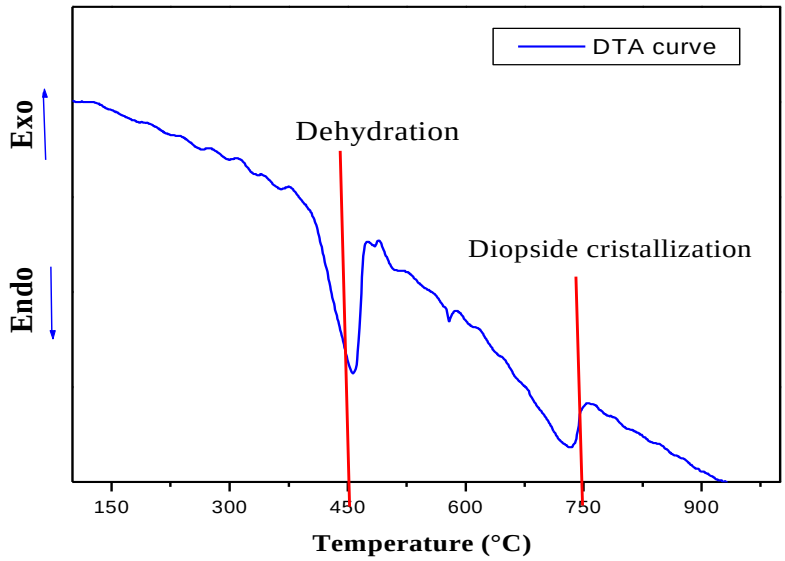


Fig.III.1. DTA curve of pure diopside samples.

Adding a small amount of sodium carbonate (0.5 wt.%) significantly improved the crystallization process. At 740°C, diffraction patterns show diopside crystallization in the Na_2CO_3 added sample **(Fig.III.2b)**, unlike the unmodified sample, which remained amorphous **(Fig.III.2b)**. This improvement is due to better densification and structural integration in the doped sample, enabling crystallization at a lower temperature.

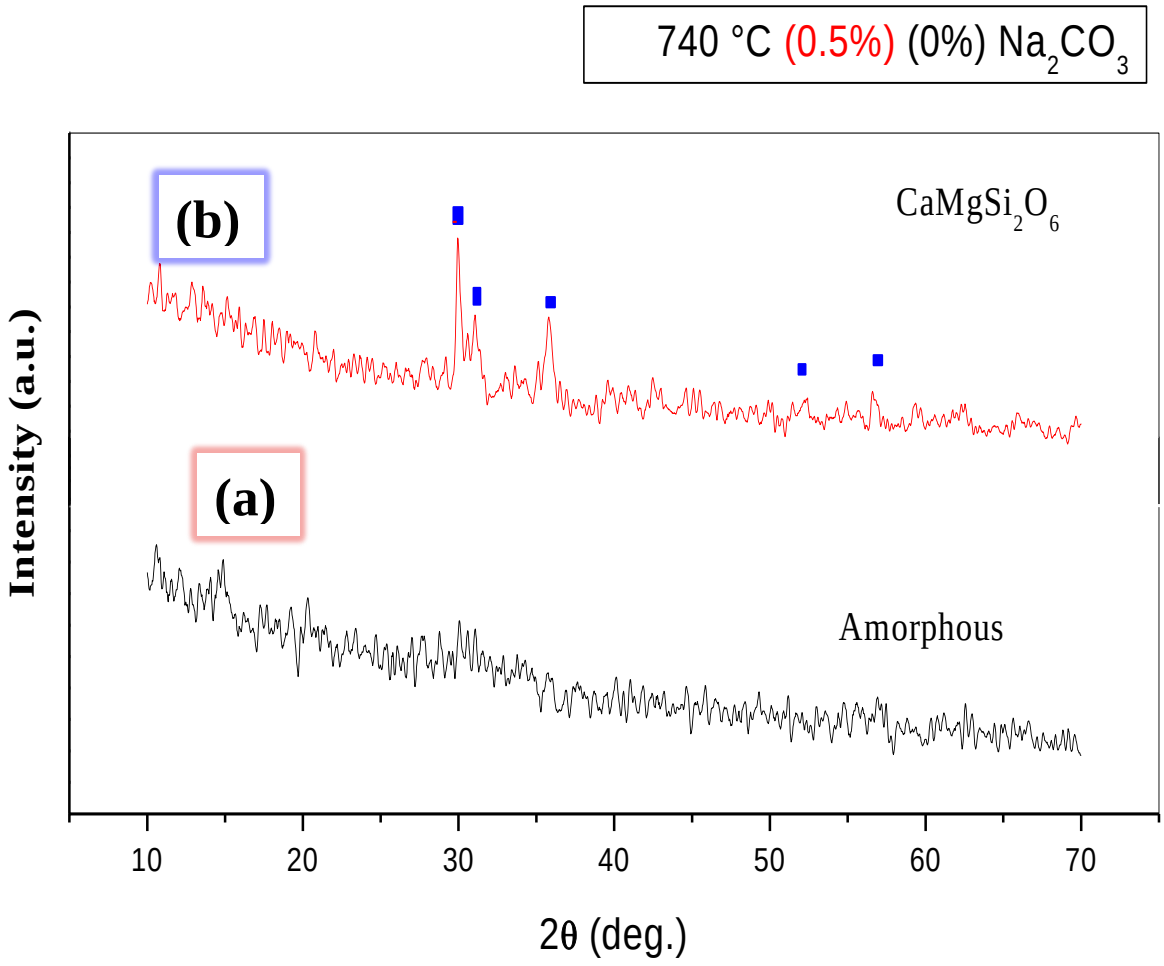


Fig.III.2. XRD spectra of pure diopside and diopside doped with 0.5 wt.% Na2CO3, calcined at 740°C for 2 h.

III-1-2 Investigating the impact of adding 0.5% Na_2CO_3 on the sintering:

Figure III.2.a illustrates the X-ray diffraction (XRD) pattern of the calcined powder at 740°C. It can be inferred that the dried powder contains an amorphous phase comprising calcium, silicon, and magnesium elements. According to **Fig.III.3.a**, the sample sintered at 1250°C without any additives consists exclusively of the mineral diopside ($MgCaSi_2O_6$, reference code: 96-101-1048). Compared to the powder calcined at 740°C, heating to 1250°C induces a reaction within the amorphous phase, resulting in the formation of pure diopside.

As shown in the XRD analysis **(Fig. III.3.b)**, the sample with an addition of 0.5 wt.% sodium carbonate also consists of pure diopside ($MgCaSi_2O_6$, reference code: 0336-900-96) without any secondary phase formation. A detailed comparison between Figures III.a and III.b indicates that the addition of sodium carbonate enhances both the intensity and sharpness of the diffraction peaks. This improvement is directly associated with an increased degree of crystallinity and crystal size

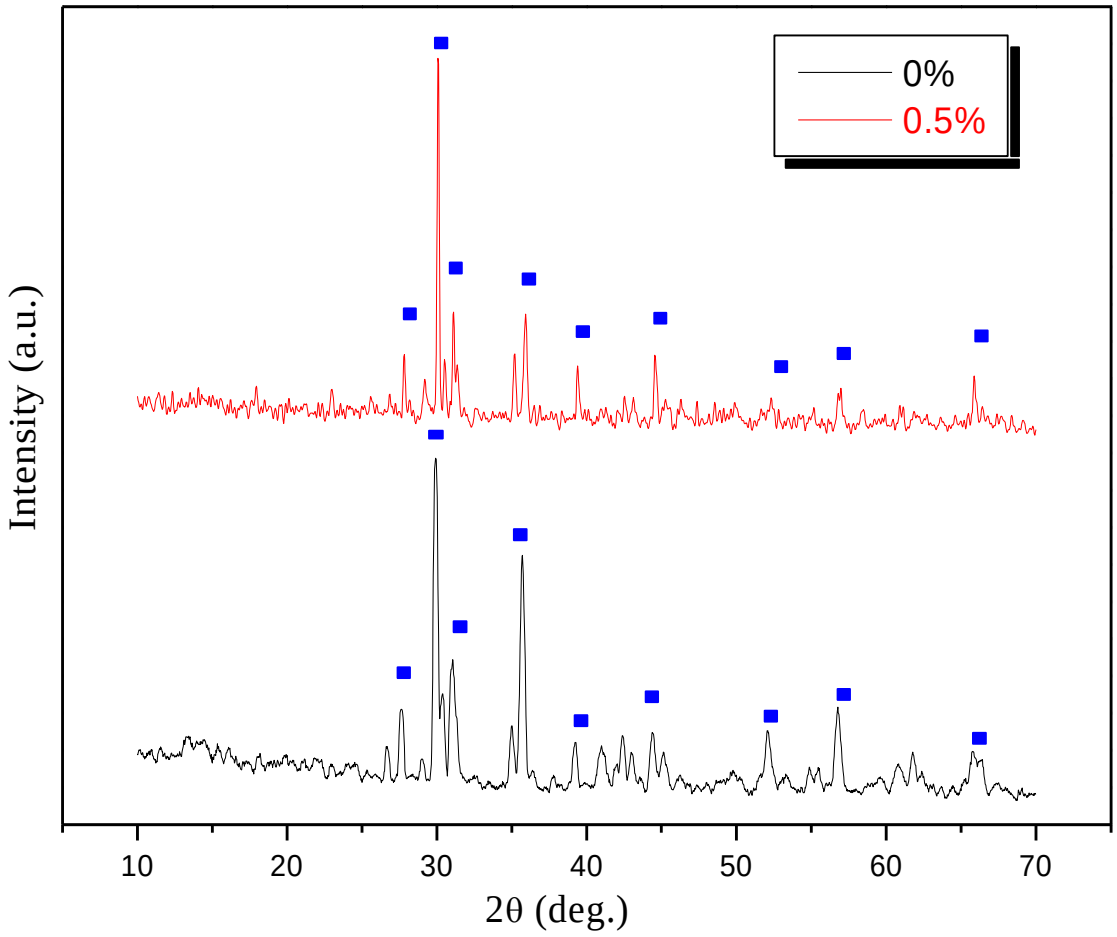


Fig.III.3. XRD spectra of pure diopside and diopside doped with 0.5 wt.% Na2CO3, sintred at 1250 °C for 2 h.

Based on calculations using the Scherrer equation, which depends on peak broadening at half maximum intensity (FWHM) of the diffraction peaks associated with diopside, crystal sizes were determined. For the sintered sample without additives, FWHM measurements were taken at prominent angles corresponding to 2θ = 30.0003°, 2θ = 30.9482°, and 2θ = 35.6893° **(Fig. III.4)**. For the sample containing sodium carbonate, the analysis was conducted at distinct diopside peaks located at 2θ = 30.0503°, 2θ = 31.1264°, and 2θ = 35.9305° **(Fig. III.5)**. The calculated crystal sizes were (22.70±1.47) nm and (50.20±2.53) nm for the non-doped and doped samples, respectively.

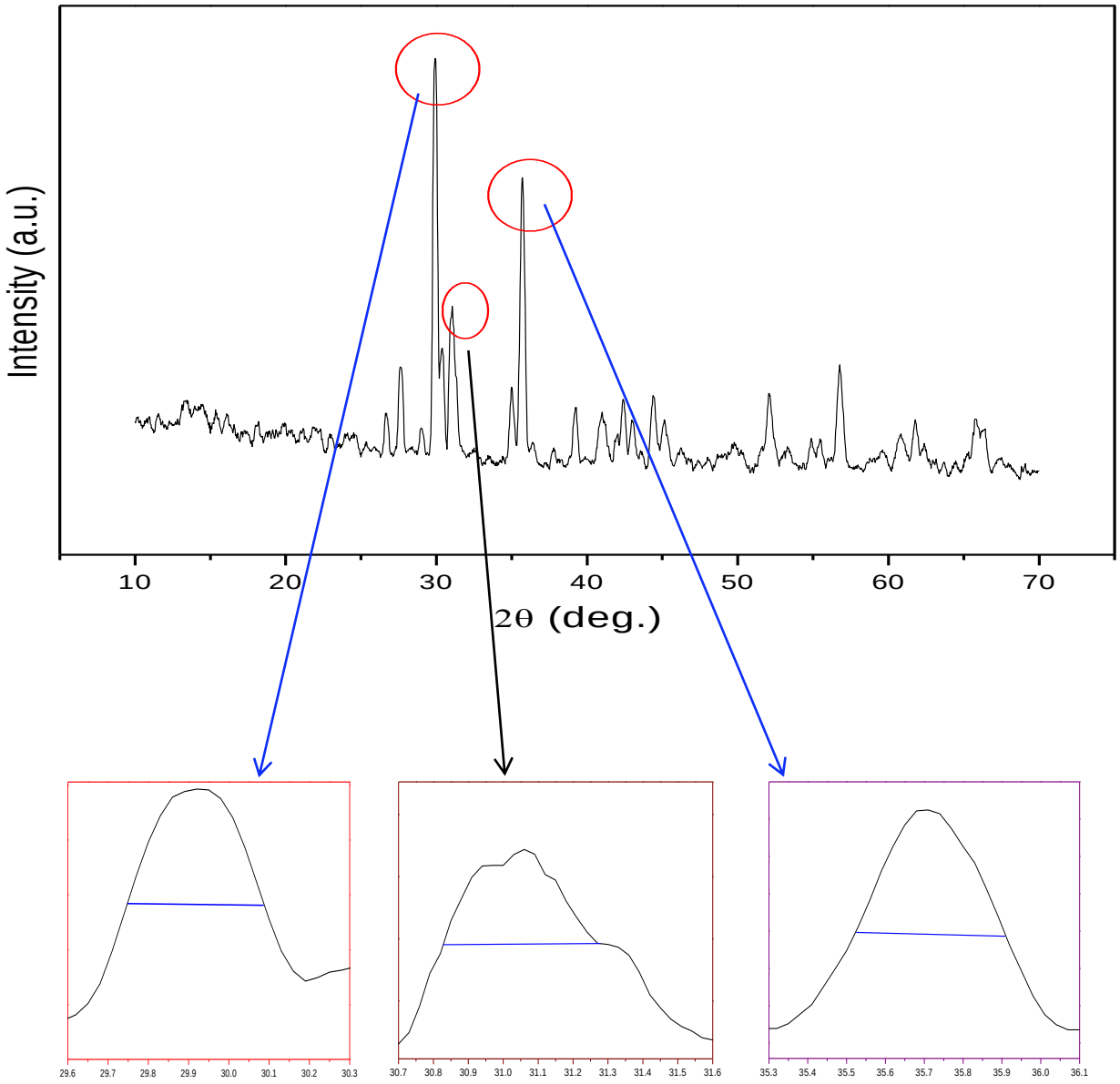


Fig.III.4. XRD spectra of pure diopside showing peak broadening for crystallite size estimation.

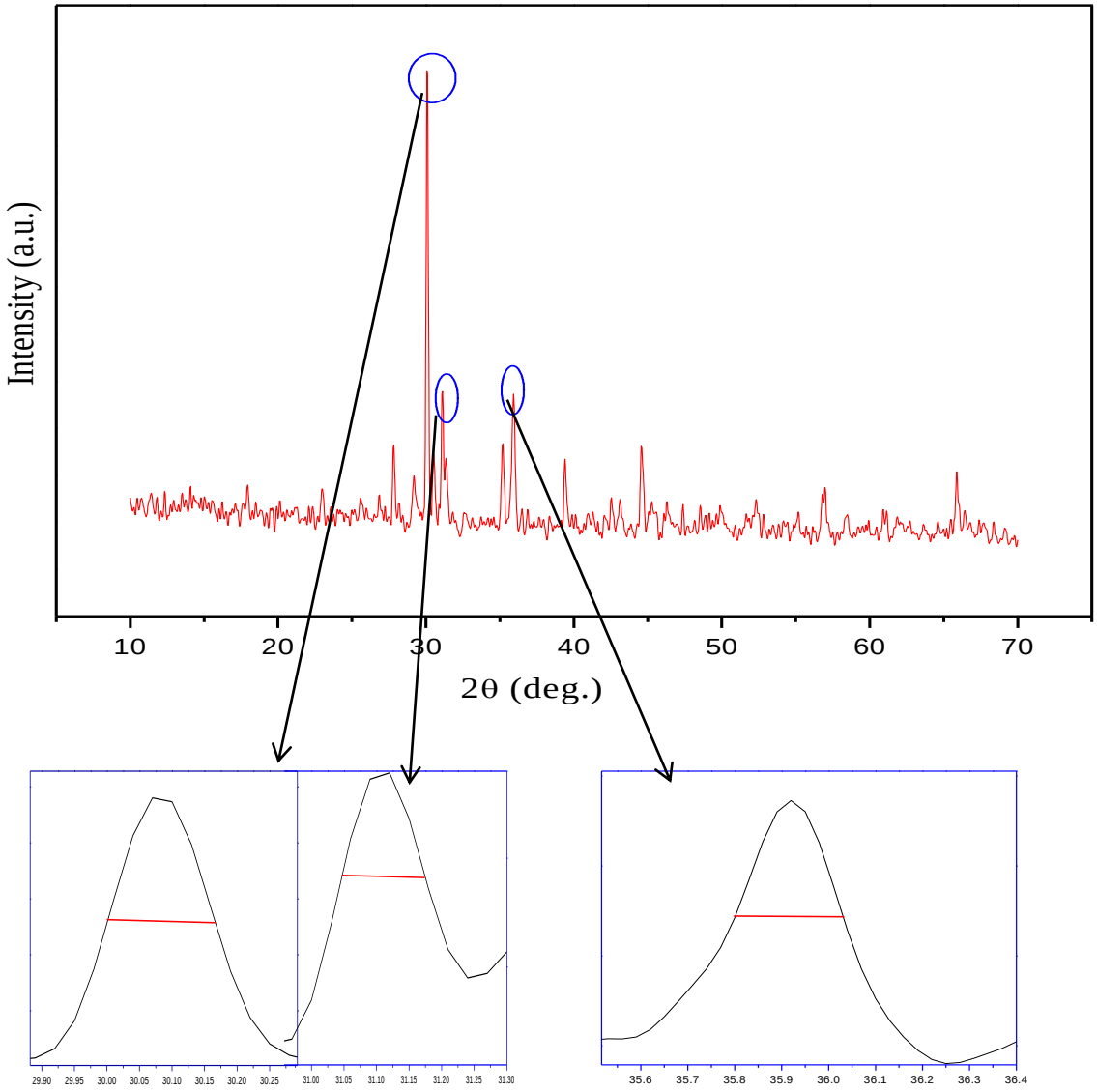


Fig.III.5. XRD spectra of doped diopside showing peak broadening for crystallite size estimation.

This enhancement can be attributed to sodium carbonate lowering the melting point of silicates, effectively achieving a relatively higher localized temperature during sintering at 1250°C. The elevated temperature promotes better crystallization and larger crystal size under identical heating conditions, explaining the observed differences in XRD peaks between the sintered samples. Additionally, this phenomenon accounts for the higher density measured for the doped sample (0.5 wt% sodium carbonate) at 3.1 ± 0.01 g/cm³, equivalent to a sintering rate of 96.88 ± 0.36% **(Table III.1)**. In comparison, samples composed of pure diopside prepared under identical conditions displayed a density of 2.76 ±0.01 g/cm³, corresponding to a sintering rate of 86.25 ± 0.36% **(Table III.1)**. This discrepancy reflects grain growth and pore elimination in the doped

sample. On one hand, the results of this study were analyzed in relation to crystal size measurements, aiming to explain the improved mechanical properties achieved by adding sodium carbonate **(Table III.1) [45]**. It is well-known that mechanical properties are closely linked to the degree of sintering; the better the sintering quality of the samples, the more enhanced their mechanical properties. Consequently, the significant role of adding a small proportion of calcium carbonate in improving mechanical property outcomes is evident.

These findings align with the sintering studies referenced in Chapter 1, further validating their consistency with established research **[33,35].**

Table III.1. Mechanical and Structural Properties of Diopside samples sintred at 1250 °C for 2 h.

1250°C	Crystallite Size (nm)	Flexural Strength (MPa)	Tensile strength (MPa)	Hardness (GPa)	Sintering density (g/cm^3)
0%	22.70±1.47	167.4 MPa	62	(4.1 ±0.1)	(2.76 ±0.01)
0.5%	50.20±2.53	191.7 MPa	71	(5.7 ±0.1)	(3.10 ±0.01)

III-1-3 Investigation the impact of adding 0.5% Na_2CO_3 on changes in chemical composition using (FTIR) spectroscopy:

To further investigate the structural characteristics of the synthesized materials and confirm the incorporation of sodium (Na) into diopside, Fourier Transform Infrared Spectroscopy (FTIR) was used to analyze the sintered samples. For pure diopside, as illustrated in **Fig. III.6a**, the FTIR spectra revealed several vibrational modes. Non-bridging oxygen (NBO) bending modes at approximately 510 and 519 cm^{-1} were identified, corresponding to the O-Mg-O bond. Sharp double peaks located at 639 cm^{-1} and 675 cm^{-1} were associated with silicate (Si–O–Si) bending modes. Additionally, prominent absorption bands were observed at 865 cm^{-1} and 965 cm^{-1}, indicating the presence of extended silicon bonds (NBO) **[24,25]**. The symmetrical vibrational modes of the Si-O-Si functional group were identified at 1041 cm^{-1} and 1058 cm^{-1}. Other significant bands included one at approximately 1635 cm^{-1} **[27]**, attributed to the bending vibrational mode of adsorbed H_2O, and a stretching vibrational band near 3493 cm^{-1}, related to moisture absorption. Furthermore, absorption bands linked to carbonate groups appeared within the wavenumber range of 1488 cm^{-1}, 1506 cm^{-1}, and 1553 cm^{-1} **[15]**.

The analysis of the pure diopside sample, derived from the prepared material without additives, showed consistency with the spectra of naturally occurring diopside. However, a notable difference was the presence of carbon-related absorption bands, likely originating from dolomite rock used as the raw material, which inherently contains carbon in its composition.

To characterize the structure of diopside doped with 0.5 wt.% sodium carbonate (Na_2CO_3) and assess the extent of sodium incorporation into the diopside lattice, the doped and sintered sample (processed at 1250°C for two hours) was examined using FTIR. The spectra for this doped sample, shown in **Fig.III.6b**, exhibited absorption bands similar to those observed in pure diopside. Non-bridging oxygen bending modes were detected at around 510 cm^{-1}, corresponding to O-Mg-O groups, along with silicate-related bending modes (Si-O-Si) at 632 cm^{-1} and 672 cm^{-1}. Additional non-bridging stretching modes for Si-O-Si groups appeared between 854 cm^{-1}, 865cm^{-1}, 911 cm^{-1} and 963 cm^{-1} **[24,25]**.

Symmetric stretching vibrations of Si-O-Si were observed at 1071 cm^{-1} and 1059 cm^{-1}. Interestingly, the characteristic absorption band for diopside around 1041 cm^{-1} was absent in the doped sample.

Notably, new absorption bands emerged in the spectrum of the doped sample that were absent in pure diopside. These bands were mainly attributed to interactions involving sodium, silicon, and oxygen. A peak at 617 cm^{-1} corresponded to asymmetric bending vibrations of an O–Si–O(Na)(H) bond **[46]**, indicating the formation of this bond within the structure. Another band appeared at 758 cm^{-1}, also linked to asymmetric bending vibrations of the same bond type. These findings confirm that sodium was successfully incorporated into the diopside crystal structure without compromising or altering its primary framework.

Figure III.6 illustrates the spectra of pure diopside alongside diopside doped with 0.5 wt.% sodium carbonate (Na_2CO_3), revealing a reduction in the intensity of absorption bands associated with the silicate group (Si-O-Si). This decrease, observed before immersion in SBF, is primarily linked to the introduction of sodium carbonate into the sample. Sodium ions (Na^+) function as network modifiers within structures containing Si-O-Si bonds, integrating into the crystalline lattice **[47,48]**. This structural modification accounts for the emergence of sodium-specific bonds in the FTIR analysis following the addition of sodium carbonate. The incorporation of sodium ions disrupts these covalent bonds, resulting in the formation of non-bridging oxygens (NBOs). Such structural changes significantly impact the vibrational spectra, as depicted in **Fig. III.6.**

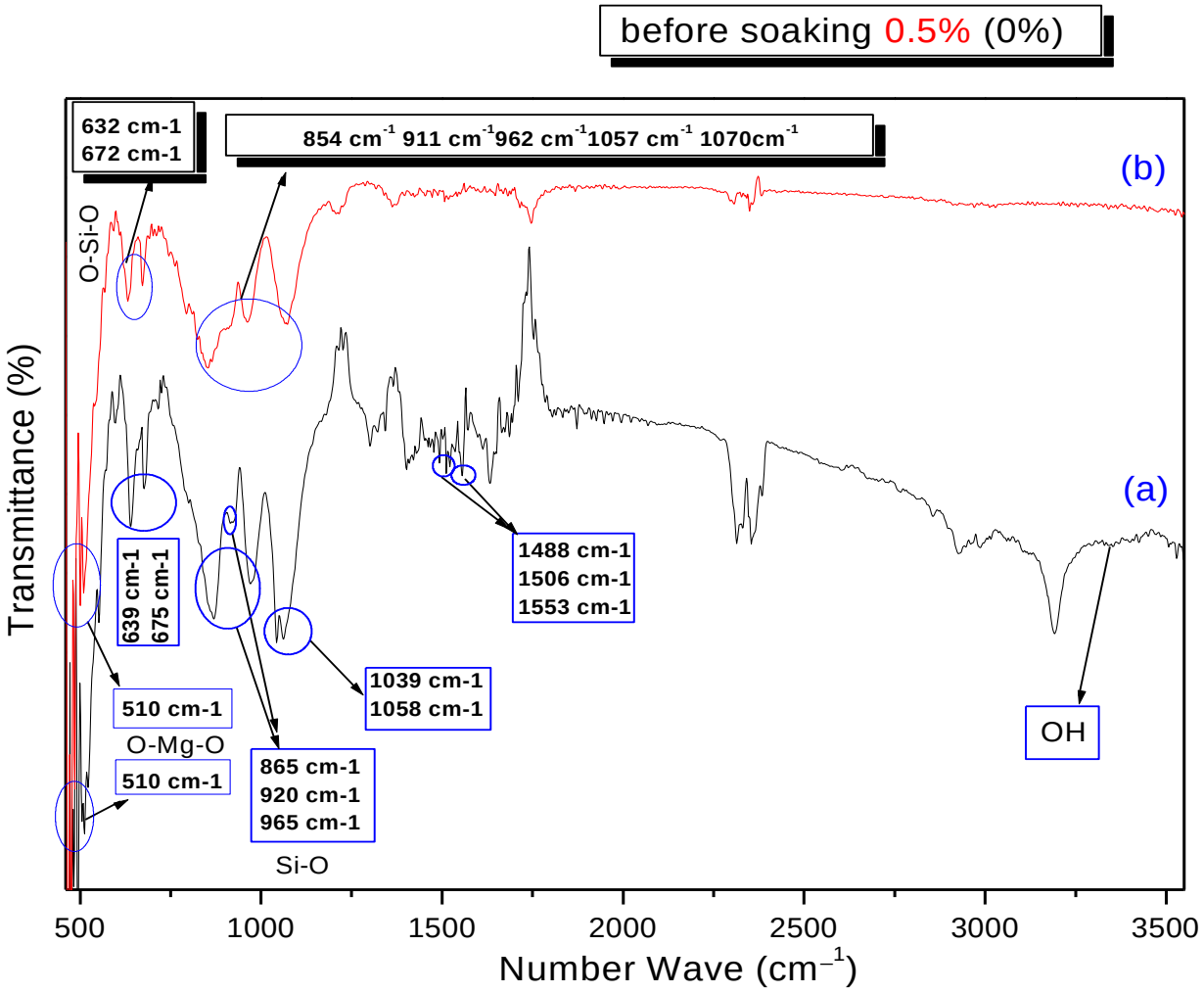


Fig.III.6. FTIR spectra of both sintered undoped (a) and doped with 0.5 wt.% Na_2CO_3 (b) samples prior to their immersion in the SBF solution.

III.2 In-vitro bioactivity assessment:

To investigate the effect of sodium activation on the bioactivity of diopside, sintered samples were immersed in simulated body fluid (SBF) for different durations (4 hours, 1, 4, 7, and 11 days) at a temperature of 37°C. Subsequently, the dried samples were analyzed using FTIR to evaluate the ability of diopside to form apatite.

III.2.1 After immersion for 4 hours in SBF:

Figure III.7a illustrates the results of analyzing a pure, sintered diopside specimen at 1250°C for 2 h, followed by immersion in simulated body fluid for 4 hours. The analysis was performed using Fourier-transform infrared spectroscopy, revealing vibrational modes similar to those observed in diopside prior to immersion. Noteworthy among these are the non-bridging bending modes of the O-Mg-O bond, identified within the wave number ranges of 473–507 cm^{-1} and 522 cm^{-1} **[27.29]**. Furthermore, sharp, double absorption peaks at 635 and 671 cm^{-1} were observed, corresponding to silica-related bending vibrations **[31]**. Absorption bands at 863 and 965 cm^{-1} confirmed the presence of extended Si-O bonds **[27]**. Additionally, absorption bands at 1038 and 1058 cm^{-1} were attributed to symmetric stretching vibrations of the (Si-O-Si) functional group **[30.31]**. Meanwhile, carbonate groups remained within the same frequency range as observed in the pre-immersed sample.

Following the immersion of a diopside sample containing 0.5% sodium carbonate in simulated body fluid (SBF) for 4 hours, FTIR analysis was conducted to examine its spectral characteristics. As shown in Fig. III.7b, there was a notable reduction in the intensity of the functional groups compared to the pre-immersion sample **(Fig.III.6b)**. Specifically, a weak absorption band corresponding to PO_4^{3-} (ν_3) appeared at 1039 cm^{-1} after 4 hours of immersion, indicating that the crystallization process of the apatite phase had not fully developed and may occur at a later stage **[49]**. Based on the FTIR results for diopside samples with sodium carbonate following immersion, it can be inferred that the material is in the early stages of apatite formation. At this point, calcium and phosphate ions gradually interact on the surface of the sample, forming initial apatite nuclei. This is evidenced by the appearance of new absorption bands associated with phosphate groups (PO_4^{3-}), which serve as clear spectral indicators of this bioactive initiation phase.

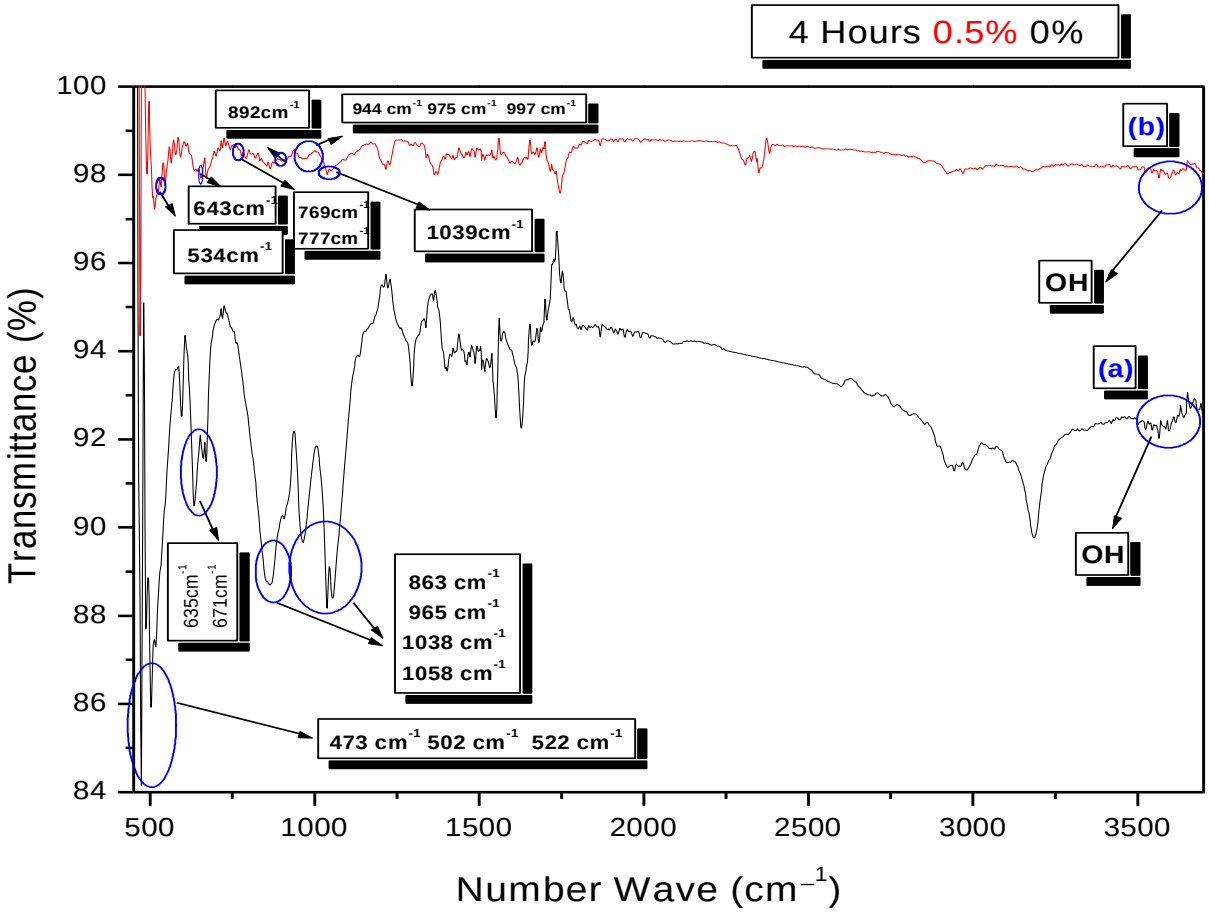


Fig.III.7. FTIR spectra of the sintered, undoped (a) and doped with 0.5 wt.% Na_2CO_3 (b) samples after immersion for 4 hours in the SBF.

Ⅲ.2.2 After immersion for 1 day in SBF:

Figure III.8 illustrates the FTIR spectra of a pure diopside sample and a sample doped with 0.5% sodium carbonate after one day of immersion in simulated body fluid (SBF). The spectrum of the pure sample **(Figure III.8a)** reveals characteristic diopside bands at 864, 963, 1037, and 1057 cm^{-1}, corresponding to Si–O and Si–O–Si vibrations, which confirm the stability of its silicate structure. Additionally, weak bands at 1412 and 1459 cm^{-1} are observed **[15]**, associated with carbonate groups (CO_3^{2-}), but they do not provide definitive evidence of apatite layer formation. A band at 1631 cm^{-1} emerges, attributed to moisture absorption linked to H_2O bound water, suggesting an initial hydration process that could relate to early stages of apatite formation. Collectively, these findings indicate that the pure sample is in the very early phases of interaction with the biological medium.

In comparison, the doped sample **(Figure III.8b)** demonstrates a notable increase in intensity near 1039 cm^{-1} **[15]**, signifying significant advancement in apatite layer formation. The bands at 1412 and 1459 cm^{-1} are more pronounced, denoting the presence of carbonate groups and supporting evidence of carbonated apatite similar to that found in natural bone. While the silicate bands remain stable, the moisture absorption bands at 3490 and 1631 cm^{-1} show increased intensity **[25.28]**, reflecting enhanced water uptake and greater deposition of the apatite layer on the doped sample relative to the pure one.

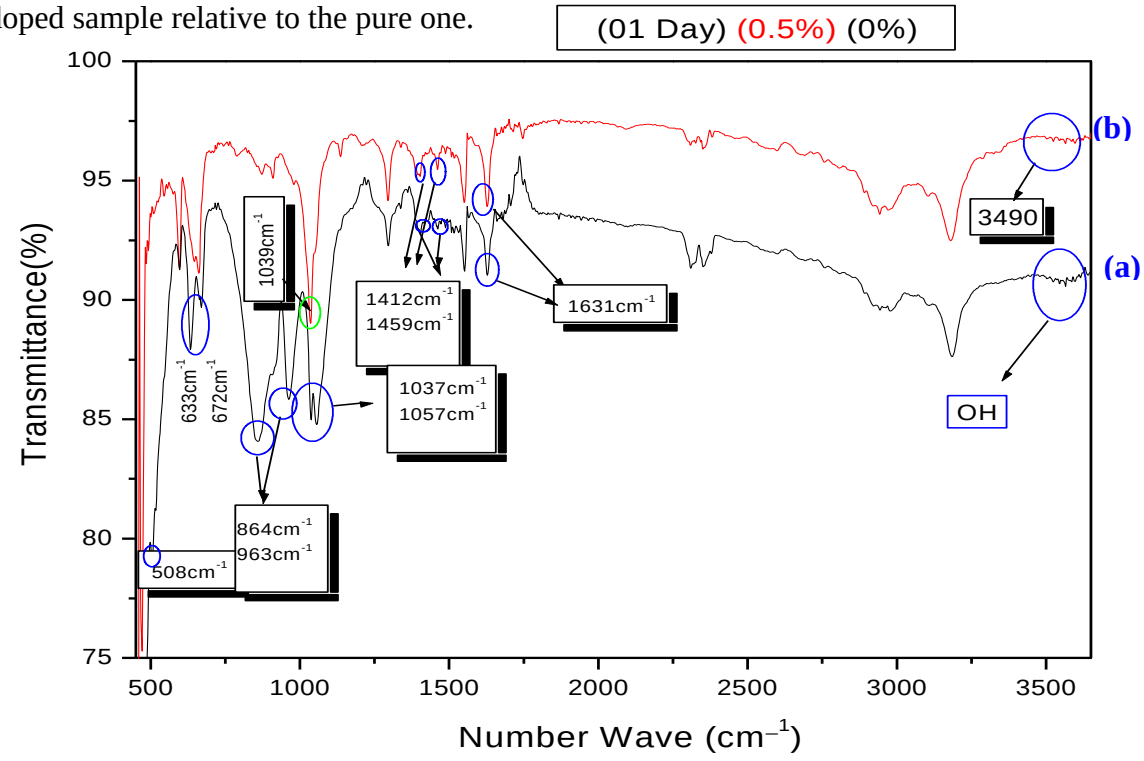


Fig.III.8. FTIR spectra of the sintered, undoped (a) and doped with 0.5 wt.% Na_2CO_3 (b) samples after immersion for 1 day in the SBF.

III.2.3 After immersion for 4 days in SBF:

After 4 days of immersion in simulated body fluid (SBF), the pure diopside sample exhibited strong structural stability, as shown by its FTIR spectrum **(Figure III.9a)**. The silica-related bands at 1038 and 1058 cm^{-1} retained their original characteristics, with minimal changes and no significant emergence of phosphate or carbonate bands. This observation suggests a slow or limited formation of an apatite layer on the sample's surface. Conversely, the 0.5% sodium carbonate-doped sample displayed notable progress in apatite formation **(Figure III.9b)**. This was evidenced by the intensified phosphate absorption band near 1039 cm^{-1} and pronounced carbonate bands at 1415 and 1453 cm^{-1}, indicating more robust growth and crystallization of carbonated apatite. Additionally, a broad and deeper absorption band around 3490 cm^{-1}, linked to O–H stretching vibrations, highlighted increased moisture uptake due to hydration processes accompanying apatite formation. Despite these surface-level changes, the persistence of silica bands indicated that the diopside crystal structure remained intact. However, the addition of sodium carbonate significantly enhanced surface interactions, improving the bioactivity of the material compared to the pure sample.

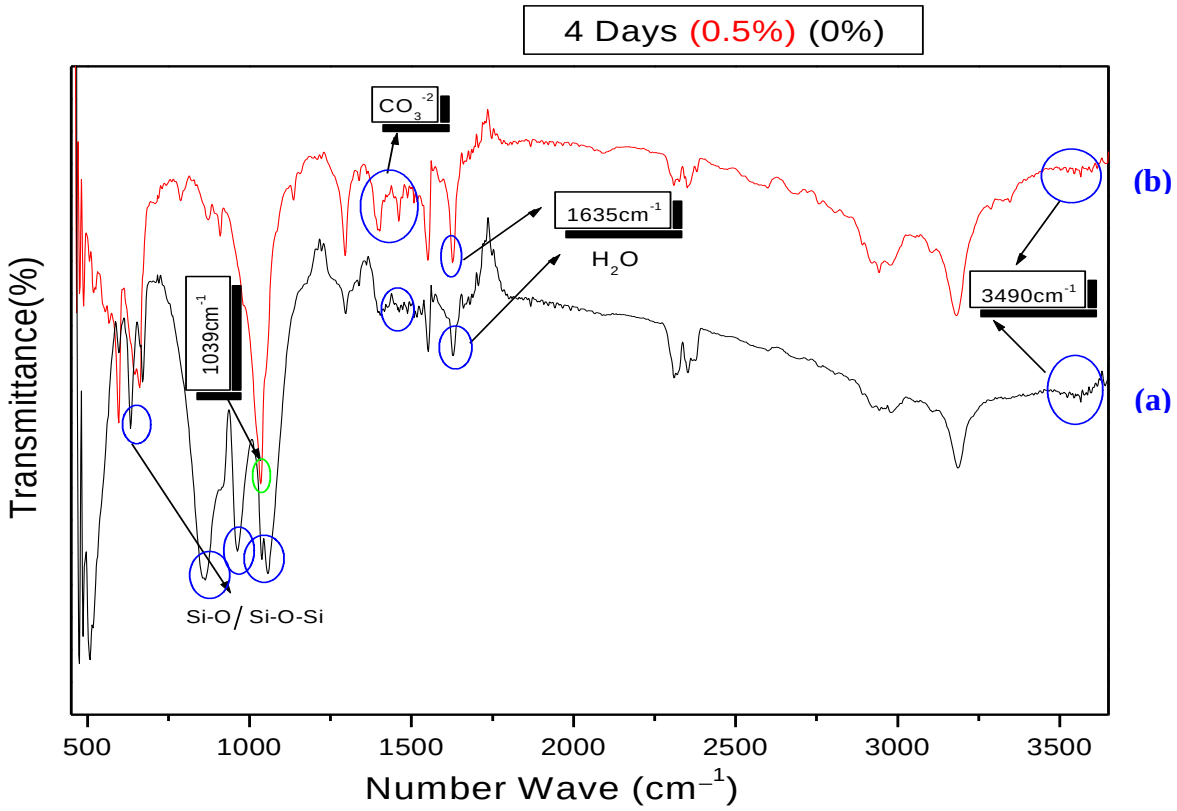


Fig.III.9. FTIR spectra of the sintered, undoped (a) and doped with 0.5 wt.% Na_2CO_3 (b) samples after immersion for 4 days in the SBF.

III.2.4 After immersion for 7 days in SBF:

In the pure diopside sample, the FTIR spectrum obtained after seven days of immersion in simulated body fluid (SBF) (Figure III.10a) shows ambiguous evidence of progressive surface interactions when compared to the results observed after one and four days. This is likely due to significant overlaps between the FTIR absorption bands of the silicate group (present in diopside) and those of phosphate, hydrogen phosphate, and carbonate groups. These overlaps make it challenging to easily differentiate between silicate and apatite species using FTIR analysis. Nonetheless, a minor shift in the silicate band from approximately 1038 to 1035 cm^{-1} was detected, indicating the initiation of surface interactions and the formation of phosphate-containing species. Meanwhile, the continued presence of other silicate bands without substantial changes confirms that the internal crystalline structure of diopside remains intact, with the observed modifications being restricted to the surface layer. Additionally, the increased intensity of the broad O–H stretching band near 3490 cm^{-1} suggests ongoing hydration and water retention within the surface layer, processes commonly associated with the early stages of carbonated apatite crystallization.

By contrast, the doped sample containing sodium carbonate **(Figure III.10b)** displayed more distinct and advanced spectral changes compared to the pure sample. The phosphate and carbonate bands appeared sharper and more intense, signifying a significant progression in apatite crystallization and the development of a denser and more organized surface layer. Furthermore, an increase in the intensity of the O–H band points to enhanced hydration, correlating with the thickening of the apatite layer. These observations underscore the role of sodium carbonate doping in accelerating the bioactive surface response while maintaining the structural stability of the original diopside matrix.

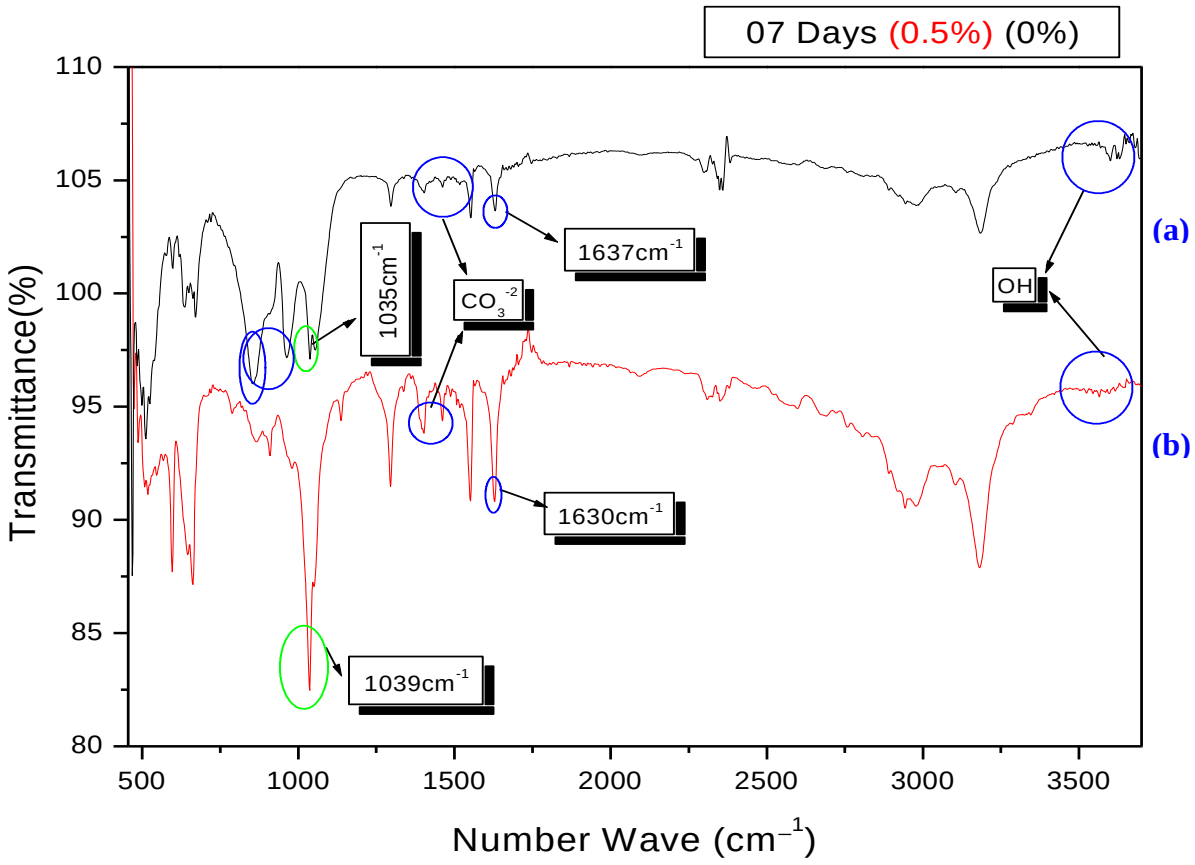


Fig.III.10. FTIR spectra of the sintered, undoped (a) and doped with 0.5 wt.% Na_2CO_3 (b) samples after immersion for 7 days in the SBF.

III.2.4 After immersion for 11 days in SBF:

In the pure diopside sample, the FTIR spectrum after 11 days **(Figure III.7a)** confirms the continuation of gradual and limited surface interactions. The silicate bands observed at approximately 965, 1057, and 866 cm^{-1} remain distinct and stable, indicating the integrity of the silicate structure is preserved. Compared to the 7 day spectrum, the slight shift of the silicate band to approximately 1035 cm^{-1} persists, accompanied by the appearance of a small new peak at roughly 1012 cm^{-1}. This peak is associated with a vibration mode of phosphate in the doped sample, signifying a mild but consistent surface interaction. These observations suggest the early stages of phosphate species formation and point to a relatively slow process of apatite nucleation. Additionally, weak carbonate bands at 1412 and 1572 cm^{-1}, along with the H_2O bending vibration at 1635 cm^{-1}, highlight ongoing hydration activity and minimal apatite development. These spectral features align with limited bioactivity, as evidenced by surface reactions occurring without significant apatite layer formation.

In contrast, the doped diopside sample containing 0.5% sodium carbonate **(Figure III.11a)** demonstrates substantial advancements in bioactivity by day eleven. Building on the notable spectral changes recorded at day seven such as intensified phosphate and carbonate bands the eleven day spectrum reveals further sharpening and strengthening of the phosphate band at approximately 1038 cm^{-1}, as well as the emergence of a distinctive peak at 961 cm^{-1} associated with PO_4^{3-} groups. These changes clearly illustrate ongoing and accelerated formation of an apatite layer. Furthermore, the carbonate bands at 1461, 1478 and 1574 cm^{-1} become more prominent, corroborating the development of a mature carbonated apatite layer on the surface. The broad and intense O–H stretching band around 3400–3490 cm^{-1}, already evident at day seven, appears even deeper and more pronounced, indicative of continued hydration and mineral accumulation within the apatite layer. Importantly, the silicate bands remain stable and distinct, confirming that while substantial surface modifications occur, the core crystal structure of diopside remains intact.

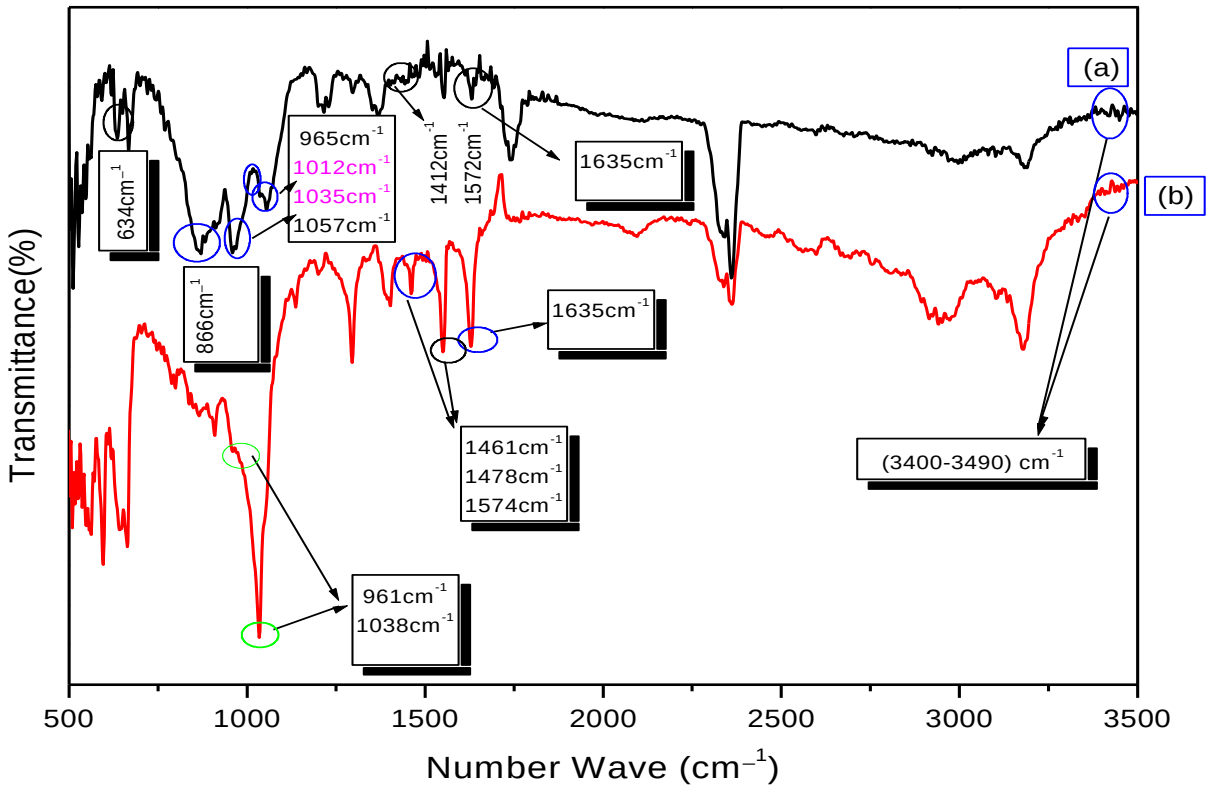


Fig.III.11. FTIR spectra of the sintered, undoped (a) and doped with 0.5 wt.% Na_2CO_3 (b) samples after immersion for 11 days in the SBF.

➢ **Conclusion:**

Fourier-transform infrared analysis of pure diopside and diopside doped with 0.5% sodium carbonate (Na_2CO_3), following immersion in simulated body fluid, revealed that sodium addition significantly enhanced the formation of a carbonated apatite layer on the sample's surface within a short timeframe. This layer showed a chemical composition closely matching biological bone apatite, specifically carbonated hydroxyapatite ($Ca_{10}(PO_4)_{6-x}(CO_3)_x(OH)_{2-x}$), demonstrating its potential suitability for biomedical applications.

The observed positive effect can be attributed to the function of Na^+ cations as network modifiers, which improve the precipitation of calcium and phosphate ions, thereby promoting apatite crystallization. Furthermore, sodium doping lowered the material's surface resistance to degradation in physiological fluids, ensuring adequate time for the development of the apatite layer. Compared to undoped samples, the presence of sodium accelerated bioactive layer formation on the surface, highlighting Na_2CO_3 as an effective and active additive.



GENERAL CONCLUSION

General conclusion

In this study, 0.5% sodium carbonate was added to diopside prepared using the solid-state reaction method. The resulting composition and bioactivity were thoroughly investigated. The findings confirmed the incorporation of sodium into diopside without the formation of any secondary phases. Improved crystallization and increased nanocrystalline size were observed under identical heating conditions when sodium carbonate was added, indicating enhanced sinterability. The ability of diopside to form apatite was significantly enhanced through sodium doping, resulting in excellent bioactivity compared to undoped powders. This improvement was attributed to the formation of a crystalline calcium phosphate-rich layer on the surface of sodium doped diopside after immersion in SBF. Ultimately, it is concluded that sodium can be considered a notable dopant for magnesium containing silicates to enhance biological behaviors, particularly bioactivity.



References

References

[1] El-Ramady, H., Alshaal, T., Omara, A. E. D.,Elsakhawy, T.A.,&Abdalla,Z. F.(2019).Soils and human creation in the holy quran from the point of view of soil science. Environment, Biodiversity and Soil Security, 3(2019), 1-9.

[2] Svinka, V., Bidermanis, L., Cimmers, A., Svinka, R. (2011) Keramzite obtaining technique. Patent of Latvia Nr.LV 14291 B.

[3] Hench, L. L. (1991). Bioceramics: from concept to clinic. *Journal of the american ceramic society*, *74*(7), 1487-1510

[4] Singh, N. B., Guin, M., & Tomar, R. (2022). Nanostructured ceramics. In Ceramic Science and Engineering (pp. 545-573). Elsevier.

[5] Dorozhkin, S. V. (2018). Current state of bioceramics. J. Ceram. Sci. Technol, 9(4), 353-370.

[6] Kattimani, V. S., Kondaka, S., & Lingamaneni, K. P. (2016). Hydroxyapatite–-Past, present, and future in bone regeneration. *Bone and Tissue Regeneration Insights*, *7*, BTRI-S36138.

[7] J. P. Marcier, G. Zambelli, W.Kurz, Introduction à la science des matériaux, presses polytechniques (1999) 16, 452,483- 484.

[8] Udduttula, A., Zhang, J. V., & Ren, P. G. (2019). Bioinert ceramics for biomedical applications.

[9] Stephano,John."Bioinert Ceramics: Advancements in Biomedical Engineering." Bioceram Dev Appl 13 (2023): 238.

[10] Pina, S., Oliveira, J. M., & Reis, R. L. (2015). Biomaterials for Tissue Engineering.

[11] Dorozhkin, S. V. (2010). Bioceramics of calcium orthophosphates. Biomaterials, 31(7), 1465-1485.

[12] Kamarudin, F. I. A. (2020). *Preliminary study on bioceramics containing gallic acid* [Master's thesis, Universiti Sains Malaysia].

[13] Heimann, R. B. (2013). Structure, properties, and biomedical performance of osteoconductive bioceramic coatings. *Surface and Coatings Technology*, *233*, 27-38.

[14] Suchanek, W. L., & Yoshimura, M. (1998). *Processing and properties of hydroxyapatite-based biomaterials for use as hard tissue replacement implants*. Journal of Materials Research, 13(1), 94–117. https://doi.org/10.1557/JMR.1998.0015.

[15] Barralet, J., Best, S., & Bonfield, W. (1998). Carbonate substitution in precipitated hydroxyapatite: an investigation into the effects of reaction temperature and bicarbonate ion concentration. *Journal of Biomedical Materials Research: An Official Journal of The Society for Biomaterials, The Japanese Society for Biomaterials, and the Australian Society for Biomaterials*, *41*(1), 79-86.

[16] Almulhim, K. S., Syed, M. R., Alqahtani, N., Alamoudi, M., Khan, M., Ahmed, S. Z., & Khan, A. S. (2022). Bioactive Inorganic Materials for Dental Applications: A Narrative Review. *Materials*, *15*(19), 6864. https://doi.org/10.3390/ma15196864.

[17] Ly, M., Spinelli, S., Hays, S., & Zhu, D. (2022). 3D printing of ceramic biomaterials. *Engineered Regeneration*, *3*(1), 41-52.

[18] Bulygina, I. N., Karshieva, S. S., Permyakova, E. S., Korol, A. A., Kolesnikov, E. A., Choudhary, R., ... & Koudan, E. V. (2024). In vitro evaluation of doxorubicin release from diopside

particles on MG-63 and HF spheroids as a 3D model of tumor and healthy tissues. *Toxicology in Vitro*, *98*, 105830.

[19] Caucia, F., Scacchetti, M., Marinoni, L., Gilio, M., Langone, A., Bartoli, O., ... & Foianini, I. (2021). An Attractive Blue Diopside from Sissone Valley, Western Alps, Italy. *Minerals*, *11*(8), 837.

[20] Nagar, R. (2011). *Preparation of diopside by novel sol-gel method using rice husk ash as silica source* (Doctoral dissertation).

[21] Sadeghzade, S., Emadi, R., & Ghomi, H. (2015). Mechanical alloying synthesis of forsterite-diopside nanocomposite powder for using in tissue engineering. *Ceramics–Silikáty*, *59*(1), 1-5.

[22] Boyd, F. R., & England, J. L. (1963). Effect of pressure on the melting of diopside, forsterite, and enstatite. Journal of Geophysical Research, 68(2), 311–323. https://doi.org/10.1029/JZ068i002p00311.

[23] E. V. Kalinkina, A. M. Kalinkin, W. Forsling, V. N. Makarov, Sorption of atmospheric carbon dioxide and structural changes of Ca and Mg silicate minerals during grinding: I. Diopside, Int. J. Miner. Process., 2001, 61, 273–288.

[24] Srinath, P., Azeem, P. A., Reddy, K. V., Chiranjeevi, P., Bramanandam, M., & Rao, R. P. (2021). A novel cost-effective approach to fabricate diopside bioceramics: A promising ceramics for orthopedic applications. *Advanced Powder Technology*, *32*(3), 875-884.

[25] S. . Zouai, A. . Fares, S. . Khuwaylid, K. . Ezzedine, and A. . Harabi, "Biological properties study of bioactive diopside prepared from local raw materials", *J. Ren. Energies*, vol. 28, no. 1, pp. 79 -, Feb. 2025.

[26] Kazemi, A., Abdellahi, M., Khajeh-Sharafabadi, A., Khandan, A., & Ozada, N. (2017). Study of in vitro bioactivity and mechanical properties of diopside nano-bioceramic synthesized by a facile method using eggshell as raw material. *Materials Science and Engineering: C*, *71*, 604-610.

[27] Sobhani, A., & Salimi, E. (2023). Low temperature preparation of diopside nanoparticles: in-vitro bioactivity and drug loading evaluation. *Scientific Reports*, *13*(1), 16330.

[28] Choudhary, R., Venkatraman, S. K., Chatterjee, A., Vecstaudza, J., Yáñez-Gascón, M. J., Perez-Sanchez, H., ... & Swamiappan, S. (2019). Biomineralization, antibacterial activity and mechanical properties of biowaste derived diopside nanopowders. *Advanced Powder Technology*, *30*(9), 1950-1964.

[29] Iwata, N. Y., Lee, G. H., Tokuoka, Y., & Kawashima, N. (2004). Sintering behavior and apatite formation of diopside prepared by coprecipitation process. *colloids and surfaces B: Biointerfaces*, *34*(4), 239-245.

[30] بن. مهنية أنفال (2023). *دراسة تشكل الأباتيت على سطح الديوبسايد*. مذكرة ماستر، جامعة الشهيد الشيخ العربي التبسي - تبسة.

[31] Cheng, L., Cai, Z., Zhao, J., Wang, F., Lu, M., Deng, L., & Cui, W. (2020). Black phosphorus-based 2D materials for bone therapy. *Bioactive materials*, *5*(4), 1026-1043.

[32] Sutharsini, U., Thanihaichelvan, M., & Singh, R. (2017). *Two-step sintering of ceramics*. InTechOpen.

[33] Anne Leriche, Stuart Hampshire, Francis Cambier. Sintering of Ceramics. Reference Module in Materials Science and Materials Engineering, Elsevier, 2017, 10.1016/B978-0-12-803581-8.10288-7. hal-03066533.

References

[34] Boch, P., & Ni, J. C. (Eds.). (2010). *Ceramic materials: Processes, properties, and applications* (Vol. 98). John Wiley & Sons.

[35] Sahoo, A. R. (2015). *Synthesis and Characterization of α-Al2O3 by Sol-Gel Process and Development of Zn-Al2O3 Composites by Powder Metallurgy Route* (Doctoral dissertation).

[36] Li, S., Wang, J. Z., Yin, B., Hu, Z. S., Zhang, X. J., Wu, W., ... & Zhang, Y. Z. (2021). Atlas of human skeleton hardness obtained using the micro-indentation technique. *Orthopaedic Surgery*, *13*(4), 1417-1422.

[37] Abdalqader, A., & Sonebi, M. (2020). Dolomitic filler in self-compacting concrete: a review. *RILEM Technical Letters*, *5*, 75-83.

[38] Sadooni, F., & Al Awadi, M. (2009). Dolomite: perspectives on a perplexing mineral. *Oilfield Review*, *21*(3), 32-45.

[39] Hsiao, Y. H., Wang, B., La Plante, E. C., Pignatelli, I., Krishnan, N. A., Le Pape, Y., ... & Sant, G. (2019). The effect of irradiation on the atomic structure and chemical durability of calcite and dolomite. *npj Materials Degradation*, *3*(1), 36.

[40] Abdullah, S. F. A., Saleh, S. S. M., Mohammad, N. F., Idris, M. S., & Saliu, H. R. (2021, November). Effect of thermal treatment on natural dolomite. In *Journal of Physics: Conference Series* (Vol. 2080, No. 1, p. 012009). IOP Publishing.

[41] Gunasekaran, S., & Anbalagan, G. (2007). Thermal decomposition of natural dolomite. *Bulletin of Materials Science*, *30*, 339-344.

[42] Mohammed, S. B., Shafi, D. S., Ghyad, Z. M., & Odeh, B. E. (2024). Synthesis of Nano-Structure Silicate Using Sol-Gel Technique. *European Journal of Theoretical and Applied Sciences*, *2*(4), 742–752.

[43] del Carmen Gutiérrez-Castorena, M., & Effland, W. R. (2010). Pedogenic and biogenic siliceous features. In *Interpretation of Micromorphological Features of Soils and Regoliths* (pp. 471-496). Elsevier.

[44] HERA (Human and Environmental Risk Assessment). (2005). *Human and environmental risk assessment on ingredients of household cleaning products: Sodium carbonate (CAS No. 497-19-8)* (Edition 2.0).

[45] Zouai, S., Guerfa, F., & Harabi, A. Sintering and Mechanical Properties of Diopside Prepared from Algerian Raw Materials.

[46] Yousef, T. B., & Abu El-Fadl, A. A. (2018). *Infrared Spectra and Thermal Properties of Sodium Silicate Solutions*. Journal of Chemical and Pharmaceutical Research, 10(2), 129–136. Retrieved from.

[47] Henderson, G. S., Neuville, D. R., & Cormier, L. (2009). The structure of silicate glasses: Insights from infrared spectroscopy. *Chemical Geology*, *262*(1–2), 123–136.

[48] Shelby, J. E. (2005). *Introduction to glass science and technology* (2nd ed.). Royal Society of Chemistry.

[49] Radwan, A. B., Mohamed, M. B., & El Sayed, M. A. (2015). Iron phosphate and hydroxyapatite composite for heavy metals removal: Preparation and characterization. *Spectrochimica Acta Part A: Molecular and Biomolecular Spectroscopy*, *150*, 43–53. https://doi.org/10.1016/j.saa.2015.05.05.